0 0 0 0 4 6 0 7 5 6 8

LBL-5706
c.1

MULLITE PHASE EQUILIBRIA IN THE SYSTEM: $CaO-Al_2O_3-SiO_2$

Victor F. Draper
(M. S. thesis)

RECEIVED
LAWRENCE
RADIATION LABORATORY
MAR 9 1977
LIBRARY AND
DOCUMENTS SECTION

October 1976

Prepared for the U. S. Energy Research and
Development Administration under Contract W-7405-ENG-48

For Reference

Not to be taken from this room

LAWRENCE BERKELEY LABORATORY
UNIVERSITY OF CALIFORNIA
BERKELEY

LBL-5706
c.1

LEGAL NOTICE

This report was prepared as an account of work sponsored by the United States Government. Neither the United States nor the United States Energy Research and Development Administration, nor any of their employees, nor any of their contractors, subcontractors, or their employees, makes any warranty, express or implied, or assumes any legal liability or responsibility for the accuracy, completeness or usefulness of any information, apparatus, product or process disclosed, or represents that its use would not infringe privately owned rights.

0 0 0 3 4 6 0 7 5 6 9

MULLITE PHASE EQUILIBRIA IN THE SYSTEM: $CaO-Al_2O_3-SiO_2$

Contents

Page

ABSTRACT v

I. INTRODUCTION 1

II. THEORY 8

A. Determination of Phase Diagrams by Diffusion Techniques . 8

1. Diffusion Couple Technique 8

2. Basis for Stable Phase Determination by Diffusion Couples 8

B. Mullite Phase Equilibria 9

1. The $Al_2O_3-SiO_2$ System 9

2. The $CaO-Al_2O_3-SiO_2$ System 10

III. EXPERIMENTAL PROCEDURE 11

A. Materials 11

B. Diffusion Experiments 13

1. Diffusion Cell 13

2. Diffusion Anneals 17

C. Quenching Experiments 18

1. Thermal History and Procedure 18

2. X-ray Analysis 19

D. Electron Beam Microprobe Analysis 20

E. Computer Analysis 23

1. Analysis of microprobe Data 23

2. Analysis of X-ray Data 24

Page

IV. EXPERIMENTAL RESULTS 25

A. Diffusion Profiles and Phase Equilibria 25

1. Sapphire-Liquid Couples 25

B. Diffusion Zone Microstructure 29

C. Phase Equilibria by Static Method of Quenching 31

1. Mullite Solid Solution in the Al_2O_3-SiO_2 System . . . 31

2. Mullite Solid Solution in the CaO-Al_2O_3-SiO_2 System . 43

D. Stable and Metastable Mullite Phase Equilibria 52

V. DISCUSSION AND CONCLUSION 57

A. CaO Effects on Mullite Phase Equilibria 57

1. Diffusion Experiments 57

2. Quenching Experiments 58

B. The Metastable Disordered Mullite Boundary for Binary Al_2O_3-SiO_2 59

ACKNOWLEDGEMENT 62

REFERENCES 63

APPENDIX I: Impurity Analysis 67

APPENDIX II: Sample Computer Input/Output of X-ray Analysis . . . 68

APPENDIX III: Sample Computer Analysis of Microprobe Data 70

0 0 0 4 6 0 7 5 7 0

MULLITE PHASE EQUILIBRIA IN THE SYSTEM:

$CaO-Al_2O_3-SiO_2$

Victor F. Draper

Materials and Molecular Research Division, Lawrence Berkeley Laboratory
and Department of Materials Science and Engineering,
College of Engineering; University of California
Berkeley, California 94720

ABSTRACT

Sapphire-liquid diffusion couples annealed in sealed molybdenum crucibles in the temperature range of 1602°C to 1787°C were analyzed by electron beam microprobe. Interfacial compositions across the phase boundaries were used to determine the stable composition range of the mullite phase field and the location of the mullite-corundum boundary. Experiments utilizing quenching methods were also conducted to establish the extent that the metastable nature of the $Al_2O_3-SiO_2$ system extended into the ternary $CaO-Al_2O_3-SiO_2$ system and to determine any solid solubility of CaO in mullite. Further evidence was obtained to confirm the recognized value of ≈82.5 wt% Al_2O_3 as the upper solubility limit for metastable disordered mullite in the binary $Al_2O_3-SiO_2$ system.

I. INTRODUCTION

The first systematic study of the Al_2O_3-SiO_2 system was conducted in 1924 by Bowen and Greig[8] who showed that, under atmospheric pressure, mullite ($3Al_2O_3 \cdot 2SiO_2$) and not sillimanite ($Al_2O_3 \cdot SiO_2$) was the only stable compound in this system. Furthermore, it was shown that mullite melted incongruently at 1828°C. The findings of Bowen and Greig were generally accepted without any serious question until 1950, when Bauer et al.[9] were successful in growing mullite single crystals by the Verneuil method. Since single crystals of incongruently melting compounds are not ordinarily produced by this method, the incongruency of mullite was thus questioned. Subsequently in 1951, Toropov and Galakhov[10] provided additional evidence that mullite melted incongruently. Since then, numerous conflicting investigations[11-24] have been conducted, some of which supported the incongruency[11-19] as originally determined by Bowen and Greig and some of which supported the congruency of mullite decomposition.[20-24] Among these, the studies of Trömel et al.[13] and Aramaki and Roy[22] were the most extensive ones. The findings of Trömel et al., in general, are in agreement with those of Bowen and Greig.[8] Aramaki and Roy's[1] diagram (Fig. 1), however, supported the congruent melting of mullite and thus led to the currently proposed mullite-corundum boundary in the ternary system under study.

A second outstanding problem of the Al_2O_3-SiO_2 system has been the determination of the stable solid solution range of mullite. Mullite normally corresponds to a composition of $3Al_2O_3 \cdot 2SiO_2$, and its solid solution range extends from 71.8 wt% to 74.3 wt% Al_2O_3. This range, however, is only realized when mullite is prepared by solid state

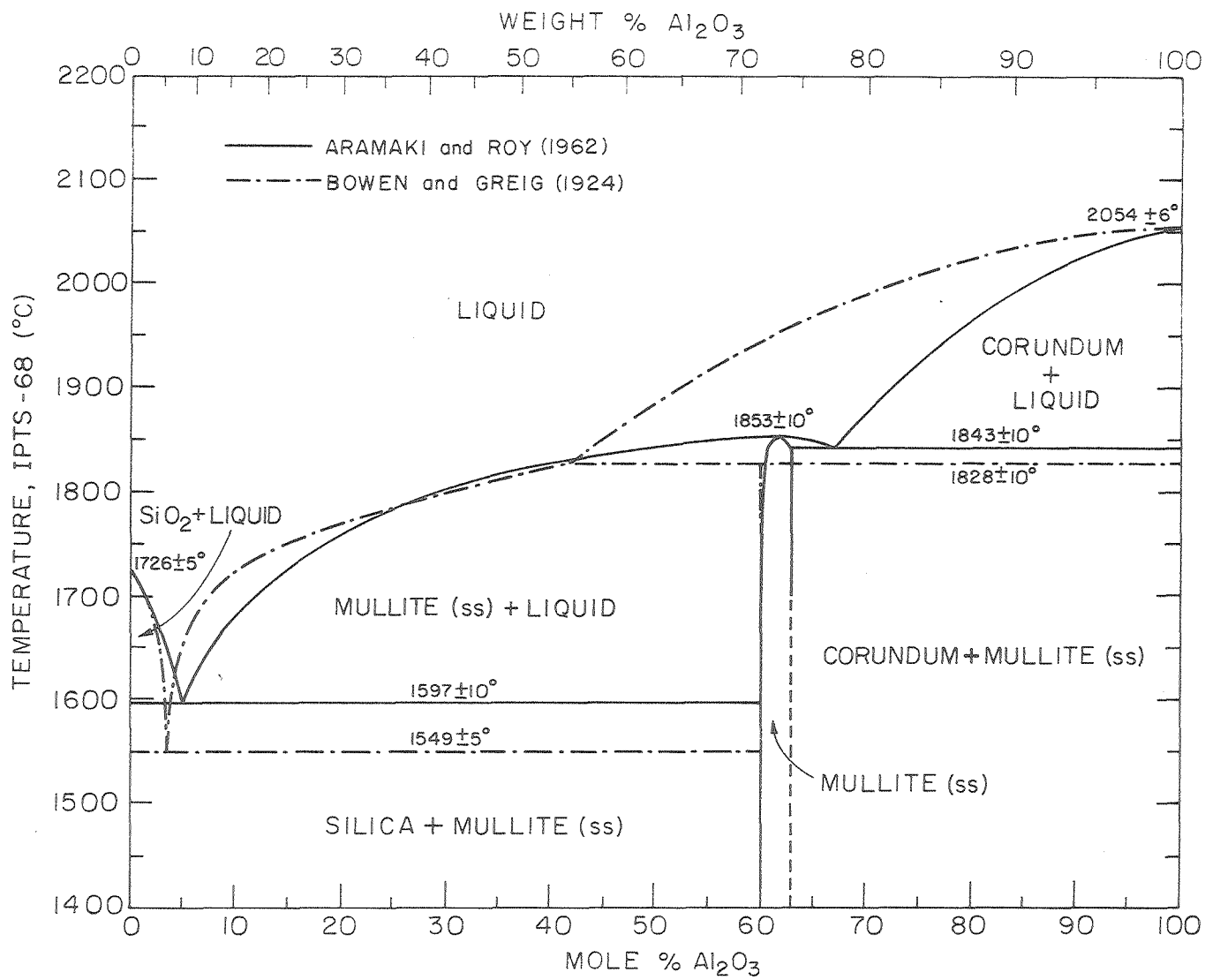

XBL 7210-7078 A

Fig. 1. Superposition of the original Bowen and Greig[3] Al_2O_3-SiO_2 phase diagram and the later revision by Aramaki and Roy.[1,22]

reactions in the presence of alumina. When solidified from a melt, the composition of mullite may extend up to 77.8 wt% Al_2O_3 ($2Al_2O_3 \cdot SiO_2$), a fact which raises the question of metastability.[2]

Most phase equilibrium studies on the Al_2O_3-SiO_2 and CaO-Al_2O_3-SiO_2 have been conducted by quenching methods[25]. Difficulties of obtaining accurate phase equilibrium data by this technique, especially in a silicate system with an incongruently melting compound, has been discussed both by Bowen[26] and Eitel.[27] Because of the sluggish nature of reactions in silicates, often non-equilibrium crystalline phases also occur which participate in metastable equilibrium diagrams. Among the investigators of the Al_2O_3-SiO_2 system, this concept was first indirectly considered by Trömel et al.[13] who argued that although the original work of Bowen and Greig reflected the stable equilibrium, it was possible to obtain a metastable congruent solidus by means of supercooling of the liquids without any alumina precipitation. This concept was rejected by Aramaki and Roy[1] on the grounds that precipitation of corundum with a relatively simple structure would occur readily when it is the equilibrium phase. Furthermore, if supercooling of the silicates with high alumina contents is indeed a possibility, any data obtained by the conventional quenching technique should be reviewed critically.

The recent revision of the Al_2O_3-SiO_2 phase diagram by Aksay and Pask[3], Fig. 2, employed both a diffusion couple technique in conjunction with quenching methods. When the diffusion couples are annealed at a sufficiently high temperature, atom mobility is enhanced, and the components of the end phases react and interdiffuse to achieve a state of chemical equilibrium.[4] If diffusion transport is the rate controlling

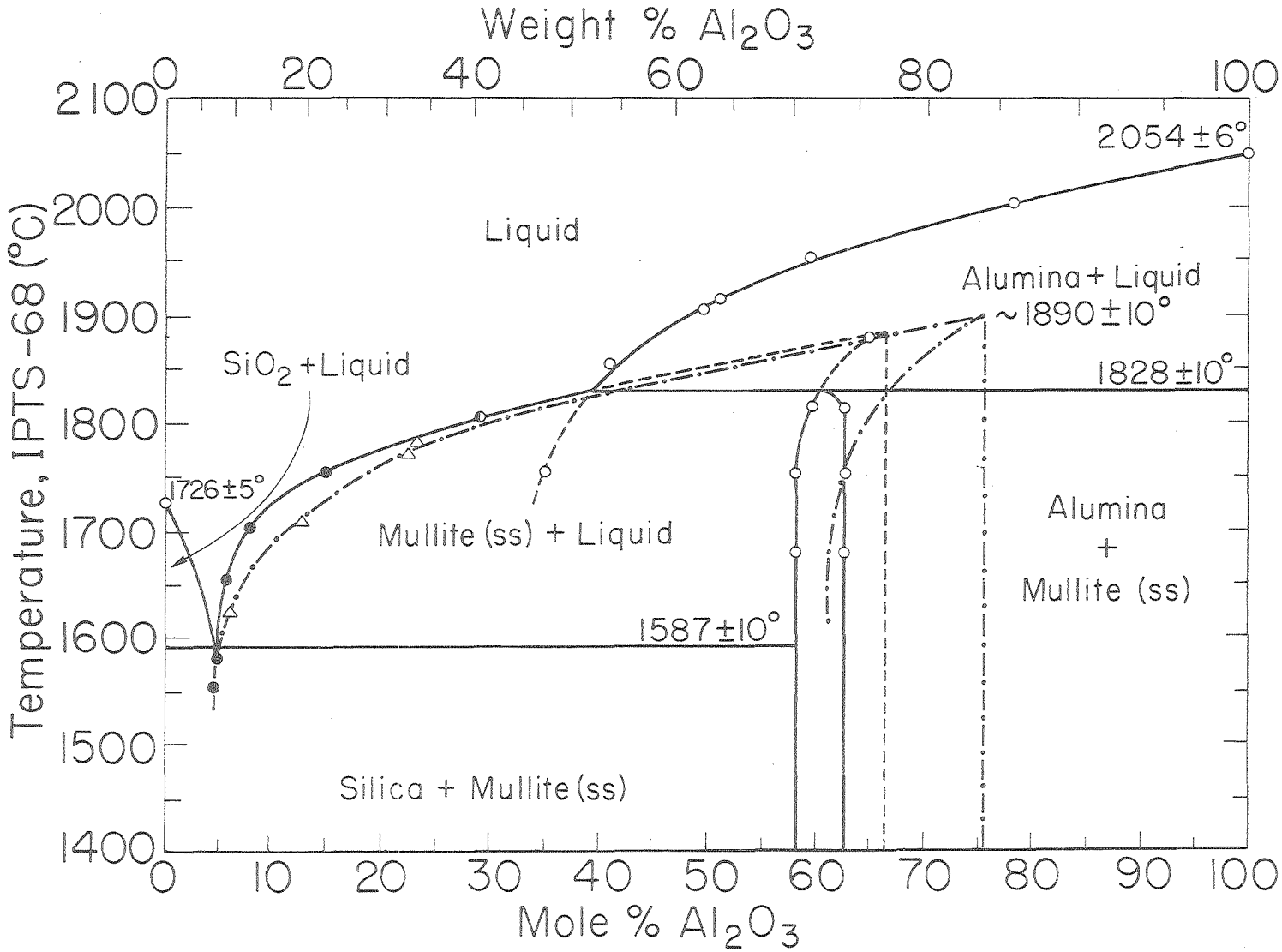

XBL 755-1377 A

Fig. 2. Composite diagram of the Al_2O_3-SiO_2 system showing the stable and metastable phases as determined by Aksay and Pask.[3]

mechanism, which is the case for the Al_2O_3-SiO_2 system, a local chemical equilibrium will exist at each interface. These interfacial compositions, then, correspond to liquidus and solidus compositions[5] and can be used to construct the equilibrium phase diagram involving the end phases of the diffusion couple.[6,7]

The currently published CaO-Al_2O_3-SiO_2 ternary phase diagram, Fig. 3, as it pertains to the mullite and corundum phase fields is based in part on the revision of the Al_2O_3-SiO_2 binary system as reported by Aramaki and Roy.[1,22] As supporting guidance[2] for the congruent melting behavior of mullite, they studied this system and the MgO-Al_2O_3-SiO_2 system to determine the location of the mullite-corundum phase boundary. Their examination of these ternary systems substantiated the congruency of mullite. As mentioned previously however, any studies involving silicate systems with a possible incongruent melting compound should be reviewed carefully when using quenching techniques. Aramaki and Roy[2] used Pt-20Rh crucibles with a maximum operation temperature of ≈1850°C and relatively short times for their quenching experiments.

In view of the quenching results of Aramaki and Roy and the diffusion studies of Aksay and Pask, three different experiments were conducted. First, and most important, was an attempt to use the diffusion couple technique to establish the stable mullite phase equilibria for this ternary system. Secondly, quenching experiments were performed to define any metastable limits on the mullite phase field as affected by the CaO additions. Also, CaO solid solubility in mullite could be ascertained. Thirdly, additional quenching experiments were conducted in the binary Al_2O_3-SiO_2 system to verify and confirm the existance of the ≈82.5

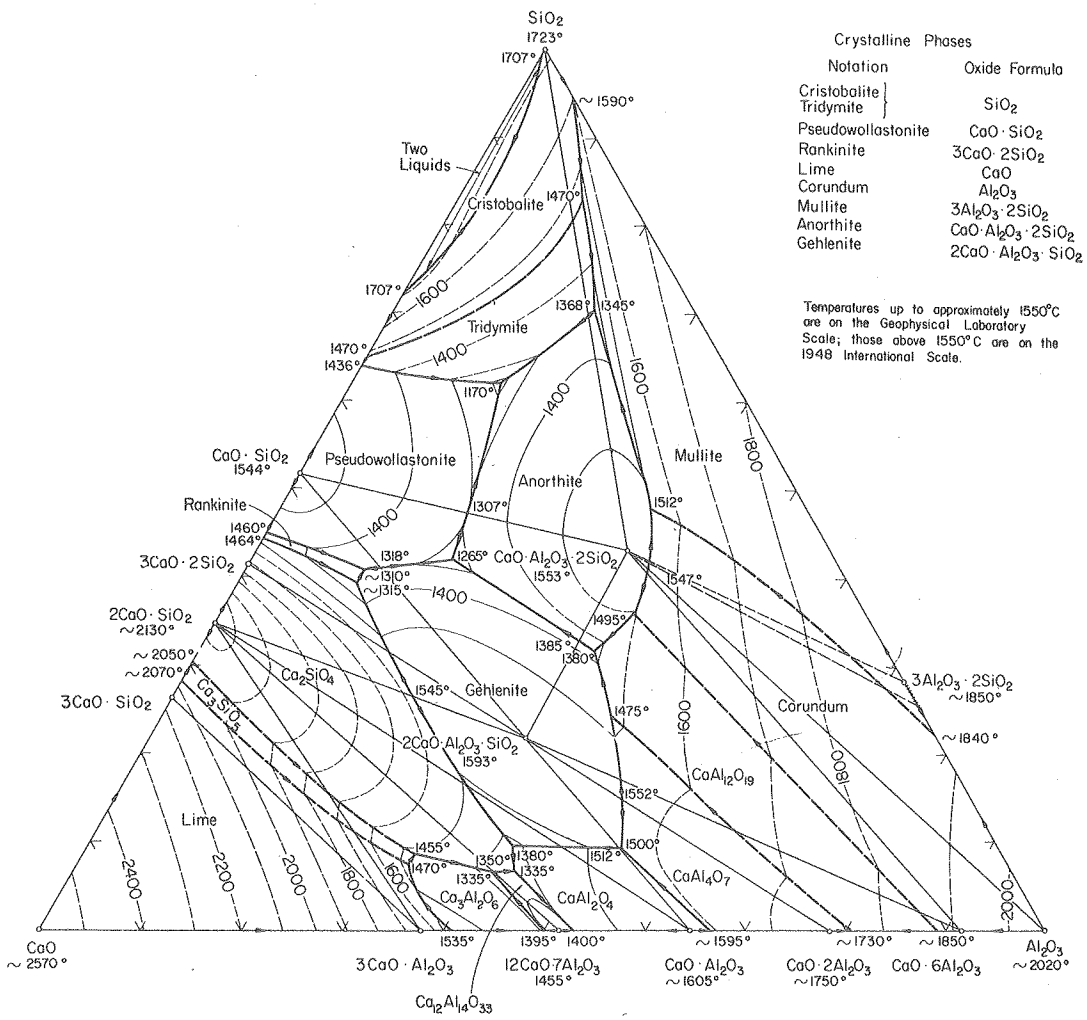

FIG. 630.—System $CaO-Al_2O_3-SiO_2$; composite.

E. F. Osborn and Arnulf Muan, revised and redrawn "Phase Equilibrium Diagrams of Oxide Systems," Plate 1, published by the American Ceramic Society and the Edward Orton, Jr., Ceramic Foundation, 1960.

XBL 764-1631

Fig. 3. Current $CaO-Al_2O_3-SiO_2$ Ternary Phase diagram[49] showing proposed mullite-corundum boundary of Arakami and Roy.[2]

wt% Al_2O_3 solid solubility limit of metastable disordered 2:1* type mullite.

*Al_2O_3-SiO_2 Molar Ratio.

II. THEORY

A. Determination of Phase Diagrams by Diffusion Techniques

1. Diffusion Couple Technique

Past work at this laboratory by Davis and Pask[28] and more recently by Aksay and Pask[3] have fully demonstrated the usefullness of the diffusion couple technique for the study of phase equilibria. When conducted in conjunction with an electron beam microprobe analysis of the cross-sections of the cooled specimens, this technique becomes an extremely powerful tool in the accurate determination of diffusion, solid solubility, isothermal and phase boundary equilibria data.

In systems where stable equilibrium conditions are not easily obtained, as in this study, obtaining accurate phase equilibria data only by the method of quenching is not sufficient. Generally, some combination of the two procedures is in order to fully realize the differences inherent in a system which readily demonstrates both stable and metastable conditions.

2. Basis for Stable Phase Determination by Diffusion Couples

When two phases of a binary, or in this study a pseudo-binary, system that are not at thermodynamic equilibrium with each other are brought into contact and annealed at a sufficiently high temperature, atomic mobility is sufficiently high so that the components of these end phases interdiffuse to achieve a state of chemical equilibrium. The diffusion of the components is in such a direction so as to eliminate any chemical potential gradient. At constant temperature and pressure, under equilibrium conditions, all the phase fields intersected by the corresponding isotherm and isobar between the end phases will form as layers

in the diffusion zone. The thickness of each layer is dependent upon its growth rate. Regardless of its thickness, however, each phase must exist in the diffusion zone in order to provide a continuous and monotonic chemical potential gradient throughout the zone. If diffusion transport is the rate controlling mechanism, a local chemical equilibrium will exist at each interface, and the motion of each interface will be proportional to the square root of the annealing time. These interfacial compositions, then, correspond to either a liquidus or a solidus composition and can be used to construct the equilibrium phase diagram involving the end phases of the diffusion couple.

B. Mullite Phase Equilibria

1. The Al_2O_3-SiO_2 System

In view of the experiments contemplated in the ternary CaO-Al_2O_3-SiO_2 system, an additional inspection of the solid solution range of disordered mullite was considered to be necessary. A number of workers[1,29] in the past have sought to establish or define this solubility range for mullite. Since the work of Aksay and Pask,[3] on stable and metastable mullite, and in view of the variation of values in the literature for this limit, a series of quenching experiments with increasing alumina content were conducted. X-ray diffraction analysis of each quenched composition was performed in order to establish its lattice parameter values. Electron beam microprobe analysis of each specimen was also undertaken so as to establish the actual crystal and matrix or liquid phase compositions.

2. The $CaO-Al_2O_3-SiO_2$ System

Due to the large solid solution range for disordered mullite in the $Al_2O_3-SiO_2$ system, it was deemed desirable to determine the solid solution range for mullite in this ternary system. Previous authors[1, 30-34] have shown no data in this respect and in order to properly establish the mullite phase equilibria any solid solubility of CaO should be demonstrated. The same procedures for analysis were used as described in the previous section.

III. EXPERIMENTAL PROCEDURE

A. Materials

Sapphire-liquid diffusion couples were prepared using alumina and prepared glasses. Highly polished single crystals (8.7 mm in diameter by 1.6 mm) of alumina (sapphire)* cut with the C-axis oriented approximately 30° form vertical were purchased.

Table I shows the compositions of the calcium-aluminum-silicate glasses mentioned above. These were prepared using high purity powders of calcined "Baker Analyzed" reagent grade $CaCO_3$*, Alcoa XA-16* reactive α-Al_2O_3 and -325 mesh Corning 7940 fused silica*. The powders were then intimately mixed with 190 proof ethyl alcohol for 24 hours in PVC (polyvinyl chloride) bottles using teflon balls. Each composition was then magnetically stirred on a hot plate at 60°C until dry, calcined at 1200°C for 24 hours to remove all remaining alcohols and hydroxyls present, with the resulting cake broken up utilizing an automated lucite mortar and pestle for 30 minutes.

The compositions were melted in large open molybdenum crucibles (2.5 cm in diameter by 4 cm) with a slightly negative helium (He) atmosphere and quenched to room temperature in ≈15 minutes.

Glass rods, 9 mm in diameter, were core drilled from each crucible, cut into 7 mm thick sections, and subjected to standard ceramographic polishing on one surface. Polishing consisted of approximately 10 minutes each on 30, 15 and 6 μm metal-bonded diamond wheels† 24 hours of vibratory†† polishing in a slurry of 6 μm diamond particles, 24 hours of

---

*See Appendix (I) for impurity analysis of all materials.
†Minnesota Mining and Manufacturing Co., So. San Francisco, California.
††Syntron Division, FMC Corp., Homer City, Pennsylvania.

Table I. Initial Glass Compositions Used in Sapphire-Liquid Diffusion Couples.

Sample Designation	Wt % Oxides CaO	Al_2O_3	SiO_2
4.01.74	8.75	30.00	61.25
4.03.74	10.50	30.00	59.50
5.01.74	7.00	30.00	63.00
8.02.75	11.25	10.00	78.75
8.17.75	13.50	10.00	76.50
8.19.75	9.00	10.00	81.00
8.22.75	18.00	10.00	72.00
8.25.75	4.50	10.00	85.50
8.30.75	1.80	10.00	88.20

vibratory polishing in a slurry of 1 μm diamond particles and 24 hours of final vibratory polishing in a slurry of 1/4 μm diamond particles.

A representative section of each glass was analyzed by electron beam microprobe for homogeneity and overall composition. They were found to be within ≃2 wt% of their starting values.

Compositions used in the quenching experiments consisted of the same high purity powders used for the diffusion couple ternary glasses. No extensive mixing was performed on these compositions. As they were to be liquified at temperature and in order to avoid any loss of material, each composition was weighed in the crucible and mechanically mixed prior to sealing. Tables II and III list the compositions, respectively, for the binary and ternary quenching experiments.

The crucibles were made with high purity molybdenum with lids which were electron beam welded and He leak checked prior to firing.

B. Diffusion Experiments

1. Diffusion Cell

The diffusion cell arrangement consisted of molybdenum crucibles containing calcium-aluminum-silicate glass disks on a sapphire substrate (Fig. 4). Molybdenum crucibles with 9.1 mm ID and ~11 mm internal height were machined from high purity rods 12.7 mm in diameter. Prior to a cell assemblage, the polished surfaces of the diffusion couple parts were checked for flatness against their counterparts to effect good bonding and prohibit the entrapment of helium or air in an irregular surface. The crucibles and the diffusion couple parts were cleaned ultrasonically in ethyl alcohol. The molybdenum crucibles were sealed around the lid by electron beam welding and He leak checked. This sealing was

Table II. Compositions Used for Quenching Experiments in the Al_2O_3-SiO_2 Binary System.

Sample Designation	Wt % Oxides Al_2O_3	SiO_2
1A	65.00	35.00
2A	70.00	30.00
3A	75.00	25.00
4A	80.00	20.00
6A	82.50	17.50
7A	84.00	16.00
5A	85.00	15.00
8A	87.50	12.50
1B	65.00	35.00
2B	70.00	30.00
3B	75.00	25.00
4B	80.00	20.00
5B	85.00	15.00

Table III. Compositions Used for Quenching Experiments in the Ternary System: $CaO-Al_2O_3-SiO_2$.

Sample Designation	Wt % Oxides		
	CaO	Al_2O_3	SiO_2
9.01.75	-	71.79	28.21
9.02.75	2.00	70.35	27.65
9.03.75	5.00	68.20	26.80
9.04.75	10.00	64.61	25.39
9.05.75	12.50	62.82	24.68
9.06.75	15.00	61.02	23.98
9.07.75	20.00	57.43	22.57
11.13.75A	10.09	29.75	60.16
11.13.75B	19.93	40.00	40.07
11.13.75C	9.99	39.90	50.10
11.13.75D	4.91	44.88	50.21
11.13.75E	9.93	49.98	40.09
11.13.75F	5.08	54.99	39.93
11.13.75G	9.98	59.56	30.46

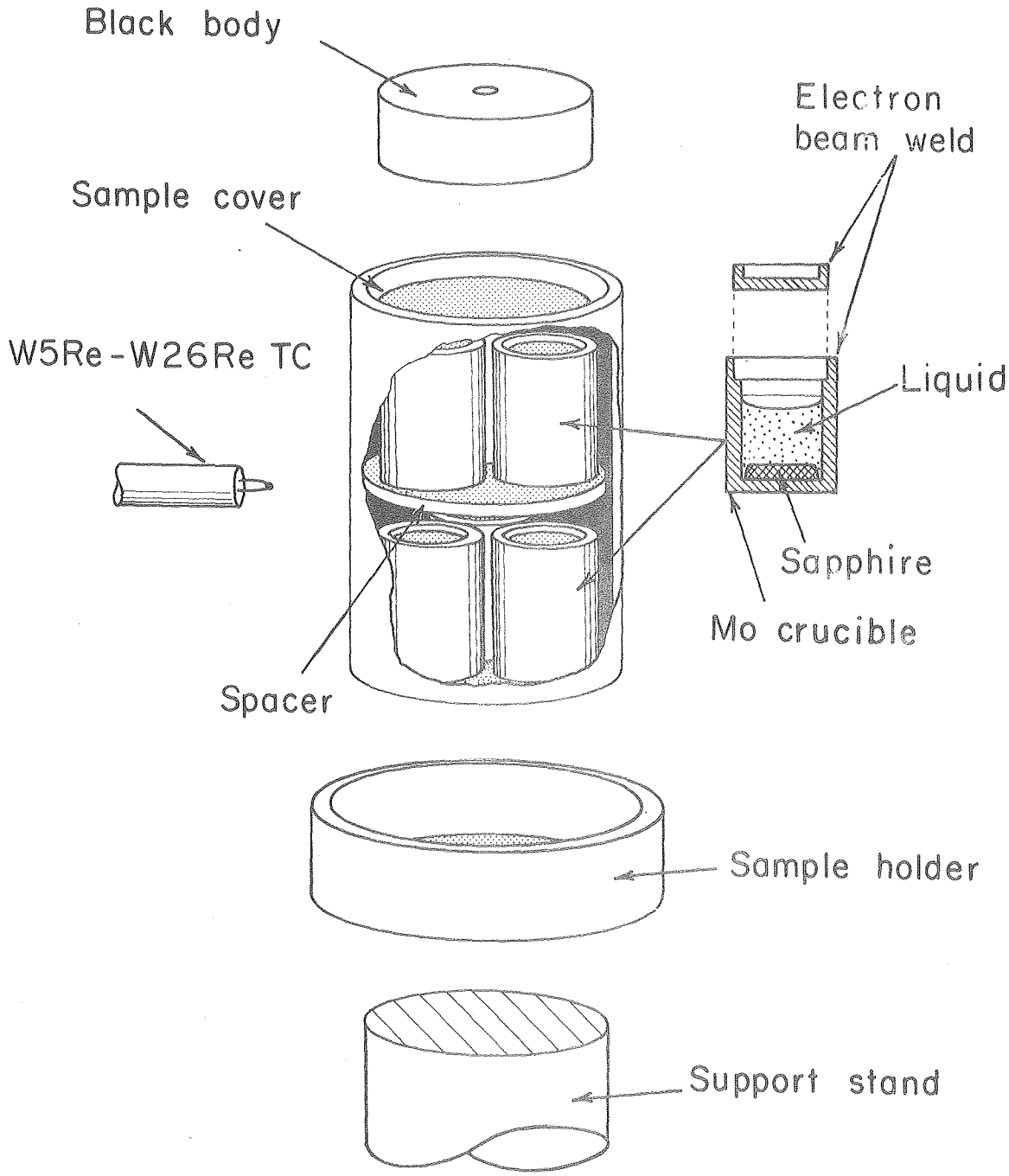

XBL7210-4191A

Fig. 4. Crucible assembly used for diffusion couples and general specimen assembly for diffusion and quenching experiments. All of the container parts are molybdenum.

necessary to eliminate silica losses by evaporation during annealing. An assembly of as many as 6 couples could be run during each annealing by stacking the crucibles with spacers in between. The crucible assembly was covered with a thick wall Mo crucible to ensure temperature uniformity.

2. Diffusion Anneals

A tantalum resistance heating furnace** with a heating zone 10 cm in diameter by 20 cm was used for all the anneals. The diffusion cell assembly as shown in Fig. 4 was placed on a Mo support stand and heated to 1200°C at 10^{-6} mm Hg. The chamber was then filled with helium slightly below atmospheric pressure, and the temperature was rapidly raised (2-3 min) to the annealing point to avoid chemical bond formation at the interface between sapphire and mullite at lower temperatures and subsequent cracking of the sapphire due to thermal expansion differences.

The diffusion anneals ranged from 1 day to 10 days, depending on the experimental conditions. The principal temperature range was from 1602°C to 1787°C. The temperature of the tantalum chamber was monitored and controlled by a Speedomax-H Recorder-Controller* and Trendtrak Programable Controller* through a W5Re-W26Re thermocouple (accuracy ± 7° at 1800°C). The specimen temperature, however, was measured separately with a optical pyrometer* (accuracy ± 10°C at 2000°C) utilizing black body conditions. The pyrometer was frequently calibrated against an NBS secondary standard pyrometer (No. 8632-C, NBS no. 4172312; accuracy

---

**Richard D. Brew and Co., Inc., Concord, NH; Model 4665-4.

* Leeds & Northrup Co., Philadelphia, Pennsylvania.

± 3°C) and at the melting point of platinum** 1772°C [35] and Al_2O_3 2054°C [36]. All the temperatures reported here are based on the 1968 International Practical Temperature Scale (IPTS-68)[35].

The diffusion anneals were completed by rapidly cooling the furnace to ≈1400°C (~1 min) to prevent excessive crystallization in the diffusion zone. Continued cooling to room temperature, however, was very slow (up to 24 hours) to avoid loss of integrity at the interface as a result of the difference in thermal expansion. The couples were subsequently sectioned parallel to the direction of diffusion, mounted in Bakelite and polished as described in Section IIIA.

C. Quenching Experiments

1. Thermal History and Procedure

Various compositions, Tables II and III, were prepared and subjected to quenching conditions. The A and B binary series were prepared from weighed Al_2O_3 and SiO_2 powders and sealed in small high purity molybdenum crucibles. Each series was raised to 2156°C, held for 15 minutes, quenched to 1804°C for A and to 1545°C for B specimens, held for 12 hours, and quenched to room temperature. Specimens 6A, 7A and 8A were not run at the same time as the remainder of the A series but were included with another run that had approximately the same thermal history.

Specimens in the 9.XX.75 ternary series were made from weighed CaO, Al_2O_3 and SiO_2 powders, sealed in small high purity molybdenum crucibles and raised to 2150°C for 1 hour to ensure liquid homogenization.

**NBS standard platinum was provided by K. S. Mazdiyasni, Air Force Materials Lab., Wright-Patterson Air Force Base, Ohio.

They were quenched to 1817°C, held for 12 hours, and quenched to room temperature. The 7 compositions lie on a tie line between 3:2 mullite and CaO in the $CaO-Al_2O_3-SiO_2$ ternary system, Fig. 3.

The 11.13.75X ternary series was made from the same oxide powders, sealed in small high purity molybdenum crucibles, and raised to 2150°C. Instead of an immediate quench, however, they were gradually cooled from 2150°C to 1400°C at the rate of 4.5°C per hour (6.8 days) using a programmable controller* and quenched from 1400°C to room temperature (≃15 min).

All the specimens were subjected to the polishing technique described in Section IIIA. Electron beam microprobe analysis was used to determine any variations in crystal and glass-matrix compositions.

2. X-ray Analysis

X-ray diffraction analysis using a Si** internal standard was performed on each remaining sections of quenched specimens after they were ground and screened through -200 mesh. Lattice parameter values were obtained from the 422, 840 and 760 X-ray peaks of mullite and refined by a least squares method as outlined in Section III, E.2. Any systematic errors occurring in X-ray diffraction vanish at $\theta = 90°$. The accuracy of the determination of lattice constants is much enhanced at higher angles. Accordingly, back reflections (θ greater than 45°) were chosen to determine the lattice parameters of mullite with the maximum accuracy. The mullite peaks occurring at planar spacings of approximately 0.826, 0.848 and 1.10Å were scanned with less restrictive collimation: 4°

---

*Leeds and Northrup Trendtrak Controller

**National Bureau of Standards, #640 Silicon.

divergence, 4° scatter collimation. A sample calculation and error analysis estimation is included in Appendix II.

A Phillips diffractometer with a Norelco monochromator detector was used which produced very high intensity copper Kd X-rays against a very low background. The scanning conditions were: 40 kV and 20 mA, 1° 2θ/min scanning rate, 1/2 in./min recording rate, 1°/4°/1° entrance to exit collimation and a time constant of 3.0 (τ).

The primary second phase with which this investigation was concerned was alumina. To ascertain its presence in quantities greater than 1%, the 113 reflection of alpha alumina was sought by slowly scanning under previously defined conditions but at a speed of 1/4° 2θ/min and τ=10. Other crystalline phases were similarly sought.

D. Electron Beam Microprobe Analysis

Weight percentage profiles of CaO, Al_2O_3 and SiO_2 from a diffusion couple experiment, Fig. 5, and the microstructure compositions of the quenching experiments were determined by an electron beam microprobe analyzer.*

The electron microprobe is a combination of a conventional X-ray tube, an X-ray emission spectrograph, a light microscope, and an electron microscope all in a common vacuum chamber. The specimen to be analyzed is bombarded by a mono-energetic beam of electrons to excite the characteristic X-radiation of the elements present in the specimen. The primary characteristic X-ray intensities emitted from the specimen and a standard may then be compared to obtain quantitative data on the concentration of each element in the specimen. Corrections for absorption,

*Model 400-S, Materials Analysis Co., Palo Alto, California.

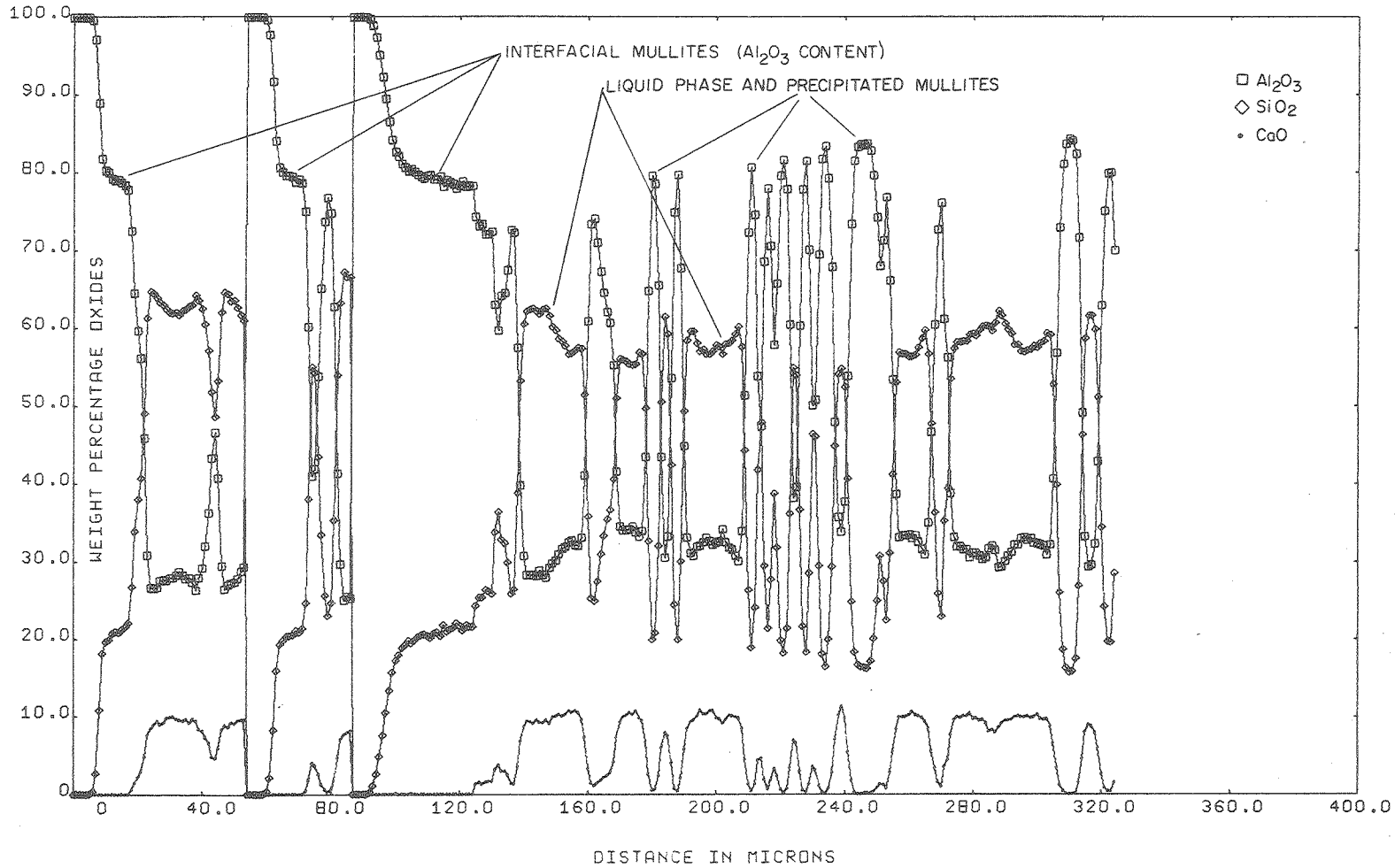

15 SEP 76
SAMPLE; 5.01.74B DIFFUSION COUPLE, 1707 C 14.26.46
XBL769-7544

Fig. 5. Representative microprobe output in wt. percent of oxides versus micron distance for a diffusion couple. 3 separate scans of the liquid phase with mullite precipitates are depicted. Large variations in Al_2O_3 for the precipitated mullites is due to their small size and the microprobe's beam interaction with the surrounding liquid phase.

fluorescence, atomic number, dead time, drift and background have to be made to improve the accuracy of the analysis.[37, 38]

Prior to electron microprobe analysis, the highly polished faces of the specimens were made electrically conductive by vapor deposition of a carbon film. Consistent film thicknesses were obtained using a technique described by Smith[39] whereby a well-polished sample of brass was observed for color changes during the deposition. Smith stated that the surface was seen to change successively from lemon yellow to orange, red, purple, blue, gray and finally to black. The purple color was easy to attain by visual control and gave good conduction. For accurate work, the standard and the unknown were placed as close to each other as possible in the carbon spray and coated simultaneously. The carbon coated specimen was then painted around the mounting material and corners with a slurry of carbon in ethanol (DAG).

All measurements were made with an accelerating voltage of 15 KeV and a specimen current of 0.025 μA. The diameter of the electron beam was 1 μm, although the volume affected was on the order of 6-7 μm^3 (cu μm).

Three spectrometers were used to record the intensities of the Ca-Kα, Al-Kα, and Si-Kα peaks simultaneously. The analyzers were curved KAP (Potassium Acid Phthalate) crystals for the Al-Kα, Si-Kα and PET (Pentaerythritol) for the Ca-Kα, all bent and ground in the Johansson mode. The detectors were of the flow proportional type containing a mixture of 93% Argon (Ar) and 7% Methane (CH_4), with a working pressure of 7 psi, and utilizing 3 μm thick mylar windows.

The profiles were obtained by traversing the electron beam along a desired path perpendicular to either the diffusion couple interface or the crystal-matrix interface. An integrated count per 10 seconds at a location was monitored by logic circuit counters and simultaneously punched on standard computer cards for subsequent introduction of computer corrections. The beam was then advanced automatically by a fixed distance (0.5 μm to 5.0 μm to repeat the same procedure).

Extensive variations in composition occurred in the liquid portion of the sapphire-liquid diffusion couples. Thus, the concentration profiles obtained by a point-beam technique were extremely rough and difficult to analyze. Davis and Pask,[28] and more recently Aksay and Pask,[3] overcame this difficulty by rapidly scanning the electron beam parallel to the interface of the couple in order to obtain an average composition. When the standards were also analyzed in this fashion, inaccuracies introduced by the decreased X-ray intensity as the beam deviates from its center may be eliminated. The scanning ranged from 40 μm to 120 μm depending on the diffusion zone inhomogeneity.

All electron beam microprobe data is an average of separate analysis on four different areas of the specimen.

Computer analysis of all electron beam microprobe data is outlined in the following section.

E. COMPUTER ANALYSIS

1. Analysis of Microprobe Data

Previous computer analyses of electron beam microprobe data, by Aksay and Davis at this laboratory, were accomplished by adaptation of

a computer program written by Frazer et al.[40] and modified for use with the CDC-7600 computer system. This program corrected for deadtime, drift, background, absorption and fluorescence. Atomic number correction was not deemed necessary for their studies since the difference between the atomic number of Al and Si is small.

This study, with the additions of CaO, required the additional correction for atomic number. A computer program written by Colby,[41] MAGIC IV, and adapted for the CDC-7600 system by this author was used. Output from MAGIC IV was then converted to wt% oxides of each of the three elements. Plots of the wt% oxides versus distance (microns), Fig. 5, were obtained using a Calcomp plotter and the necessary plotting routines. Appendix III contains a sample analysis.

2. Analysis of X-ray Data

Least squares refinement of X-ray diffraction data was facilitated by using a program originally written by Burnham,[42] LCLSQ, and also adapted for use with the CDC-7600 by this author.

Input data required was unit cell type, wavelength of the X-rays, initial lattice parameters (usually obtained from an ASTM powder file card), measured 2θ values, their Miller indicies and the desired number of iterations on each parameter. A representative input and the computed output is presented in Appendix II.

0 0 0 4 0 0 7 5 8 3

IV. EXPERIMENTAL RESULTS

A. Diffusion Profiles and Phase Equilibria

1. Sapphire-Liquid Couples

The experimental conditions of the diffusion anneals in the temperature range of 1602°C to 1784°C and the resulting overall interfacial compositions are outlined in Table IV. These are values for a large area at the interface including the liquid and crystal compositions. Such overall values correspond to liquidus compositions in equilibrium with sapphire needed for isotherm positioning. The initial liquid compositions were presented in Table I. Minimum annealing time was considerably longer (at least 24 hrs) than the time needed to attain thermal stability in the furnace (≈30-60 seconds). The composition of sapphire at the diffusion couple interface always corresponded to that of pure Al_2O_3 since the solubility limit of CaO and SiO_2 in the sapphire substrate was below the detection limit of the electron beam microprobe.

Previous work by Davis[28] and Aksay[3] on sapphire-fused silica diffusion couples noted the difficulty in growing a mullite layer at the interface due to mullites' rapid dissolution rate in unsaturated silica. When they replaced the silica portion of the couples by melts with compositions corresponding to that of the mullite liquidus, the intermediate mullite layer could be grown to a thickness (>10μm) suitable for electron beam microprobe analysis.

The experimental conditions listed in Table IV and the composition of the melts, Table I, were used in hopes of bracketing the stable mullite primary phase field in the ternary phase equilibrium diagram and ease the time requirements for any stable mullite layer growth. As

Table IV. Average Interfacial Compositions* Wt% Oxides of the Sapphire-Liquid Diffusion Couples (Crystal and Liquid Phases) for Isotherm Positioning.

Specimen Designation	Temp°C IPTS 1968	Time (Min)	Wt% Oxides CaO	Al_2O_3	SiO_2	Phases# Detected
4.01.74A	1784	8450	6.17	34.45	59.37	Mullite
4.03.74A	1784	8450	6.87	40.33	52.80	Mullite
5.01.74A	1784	8450	4.98	40.34	54.68	Mullite
4.01.74B	1707	2880	8.31	39.63	52.06	Mullite
4.03.74B	1707	2880	10.67	38.08	51.16	Mullite
5.01.74B	1707	2880	7.21	36.32	56.47	Mullite
4.03.74C	1602	1440	11.01	33.99	55.01	Mullite
5.01.74C	1602	1440	6.12	28.96	65.03	Mullite

#By X-ray diffraction in the liquid zone.

*Averages were determined by sweeping the electron beam over an 80 μm line at the interface and advancing it at 1 μm steps into the liquid zone.

an additional aid to enable a reasonable prediction of the temperature and composition requirements for the diffusion anneals, two pseudo-binary diagrams, Fig. 6, were prepared by mapping into a two-dimensional plane a tie-line between corundum and a melt of the composition corresponding to that of specimen 8.02.75. This tie-line also intersects the composition point of specimen 4.01.74. The temperature isotherms of these pseudo-binary diagrams were obtained by repositioning of the end-points of the ternary isotherms utilizing the binary Al_2O_3-SiO_2 data of Aksay and Pask[3] and the $CaO.6Al_2O_3$ phase field data of Gentile and Foster.[50] A reasonable estimate was then made as to the location of these isotherms on the liquidus surface of the mullite phase field in the ternary diagram.

The upper diagram in Fig. 6 was constructed based on the proposed location of the new mullite boundary (incongruency) whereas the bottom diagram was constructed on the basis of Aramaki and Roy's[2] proposed mullite boundary (congruency).

The important difference between these two pseudo-binaries is the temperature range of 1730°C to 1840°C. The presence of mullite in this range, after a diffusion anneal, would indicate that it melted congruently; if absent, the incongruency of mullite. Experimental evidence would thus be available to support the position of the mullite-corundum boundary.

Mullite was detected in every diffusion anneal, which indicated that mullite had a congruent melting point. However, after electron beam microprobe analysis of the interfacial layers, it was found that all of these mullites had compositions similar to the mullite precipitated from

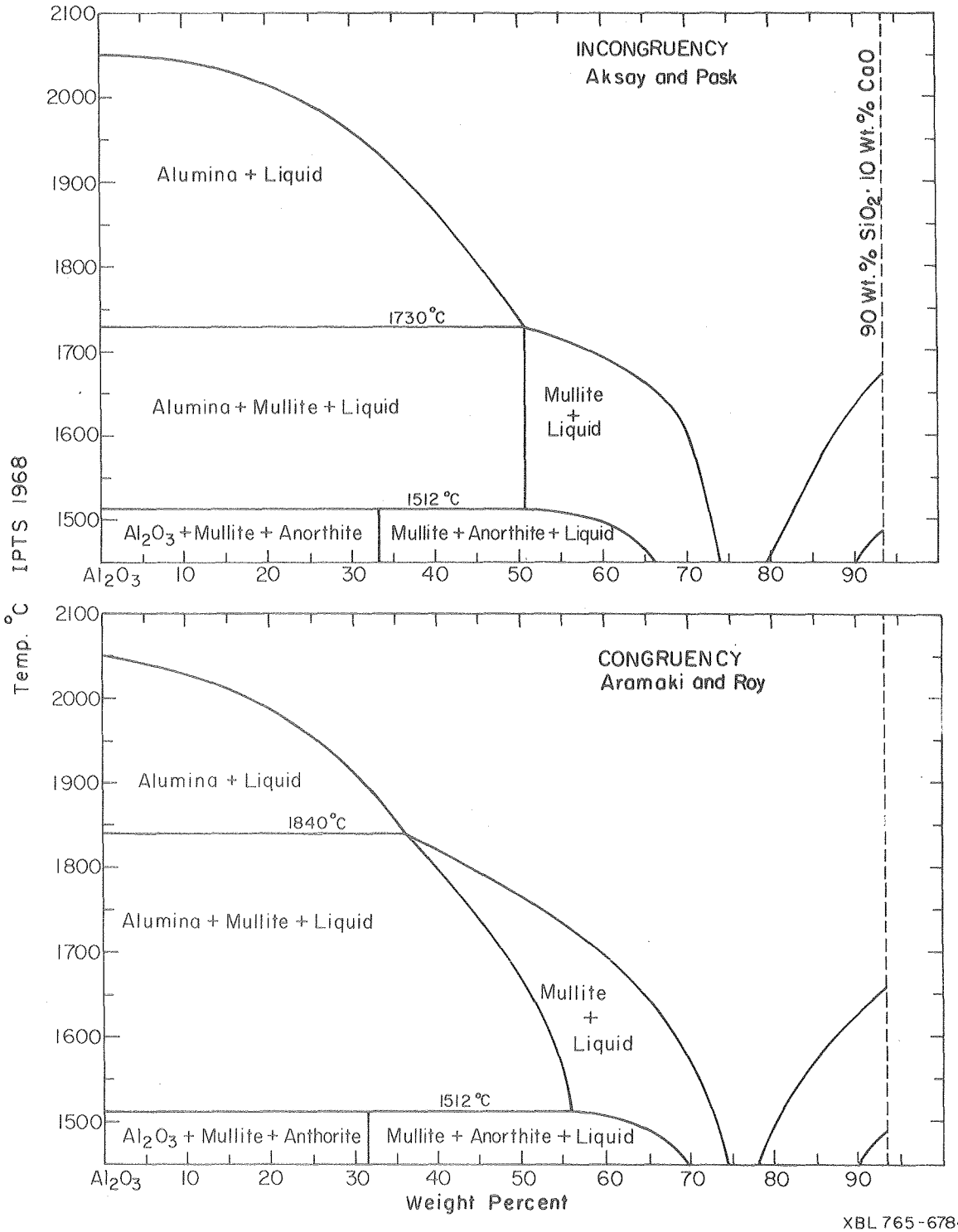

Fig. 6. Pseudo-binary systems constructed from Al_2O_3 and specimen 8.02.75 composition tie-line in the $CaO-Al_2O_3-SiO_2$ ternary phase diagram. Top figure assumes the mullite-corundum boundary based on work by Aksay and Pask[3] (incongruency), while the bottom figure is based on an Aramaki and Roy[2] revision (congruency).

the liquid phase during cooling. The following section will elaborate on this aspect.

Results from diffusion anneals with the 8.XX.75 series were uninterpretable. Considerable inhomogeneities in the diffusion zones did not lend themselves to analysis and therefore no conclusions could be formulated.

B. Diffusion Zone Microstructure

Typical diffusion zone microstructures of the sapphire-liquid couples annealed at 1707°C are shown in Fig. 7. The Al_2O_3 content of the mullite grains as determined by electron beam microprobe analysis never corresponded to the stable composition of mullite of the 3:2 type as presented in Fig. 2, but was always rich in Al_2O_3 and varied between 75.2 and 78.2 wt% Al_2O_3.

Formation of mullite with alumina contents higher than the limits outlined in Fig. 2 occurs only when it is solidified from a melt. The composition of this mullite of the 2:1 type generally is close to 77.3 wt% Al_2O_3 although values as high as 82.57 wt% Al_2O_3 have been reported.[29] Precipitation of mullite with alumina contents higher than the solidus composition outlined in Fig. 2 was also observed by Davis and Pask[28] and Aksay and Pask.[3] Davis and Pask suggested that the composition of the melt was responsible for the composition of the precipitated mullite. This point will be expanded on further in the discussion section on quenching experiments in the Al_2O_3-SiO_2 system. The fact that the composition of the precipitated mullite clearly differs from that of the mullite layer grown at the sapphire interface[3] serves as a useful criterion in the differentiation of mullite grown at temperature

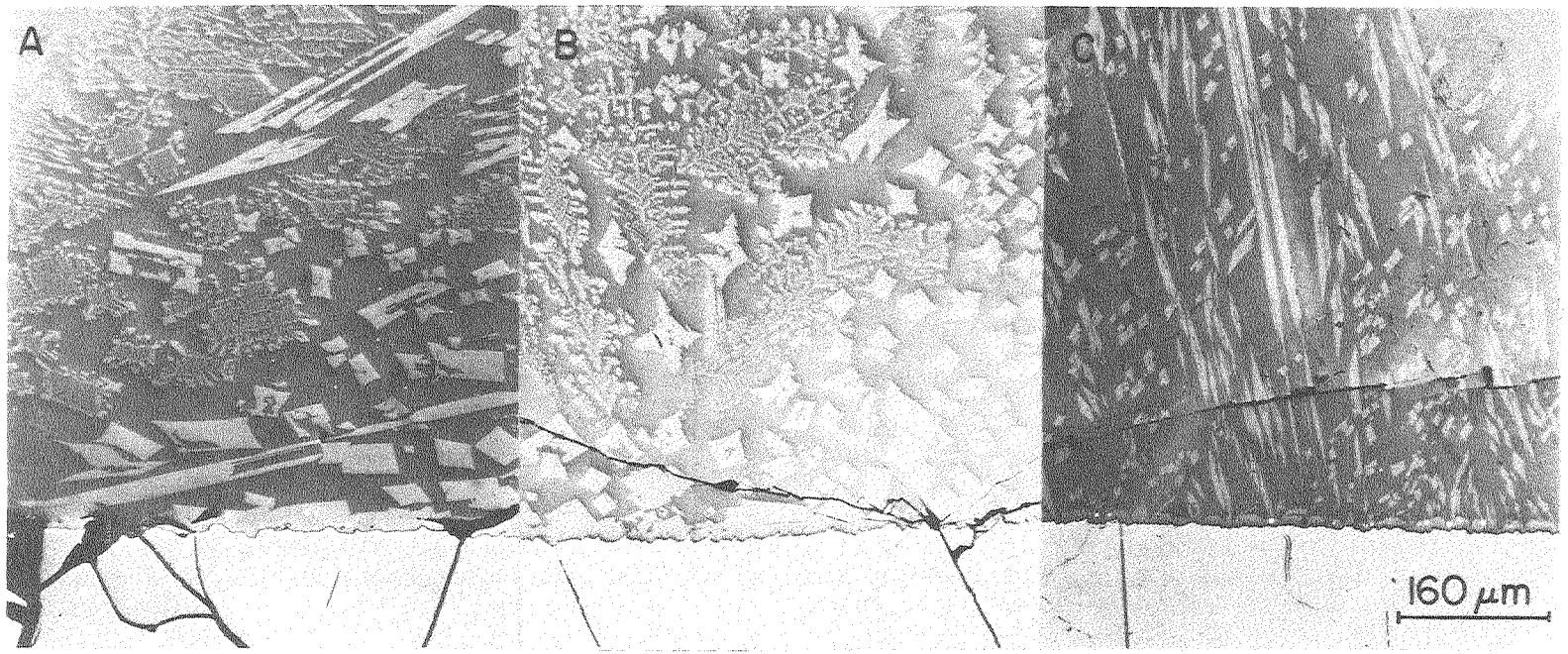

XBB767-6002

Fig. 7. Interference-contrast micrographs of the diffusion zone between sapphire (bottom) and various liquids (top) annealed at 1707°C for 172.8×10^3 sec (2 days). a) liquid 4.03.74B, b) liquid 4.01.74 B, c) 5.01.74B. The mullites present in the upper portion of the diffusion zone precipitated upon cooling as did the layers at the sapphire interface.

from mullite precipitated during cooling.

In all the diffusion anneals, the sapphire interface of the couple is covered with essentially a continuous mullite layer, Fig. 7. The composition of this layer was constant for each couple and was approximately the same as the precipitates in the liquid zone above the interface. The compositions of these mullite layers are presented in Table V along with the average composition of the precipitated mullite crystals. From the similarity in composition, and its similarity to the 2:1 type of mullite, it is concluded that this layer did not grow at temperature but precipitated at the sapphire interface during cooling.

At no time was any mullite detected that had a composition within the stable phase field of the 3:2 type mullite.

C. Phase Equilibria by Static Method of Quenching

1. Mullite Solid Solution in the Al_2O_3-SiO_2 System

Compositions spanning the possible solid solution limits of stable 3:2 type, metastable ordered and metastable disordered 2:1 type mullite as depicted in Fig. 2, with the wt% oxides of each component are shown in Table II. The A series was melted at 2156°C for 15 minutes, quenched in He to 1804°C, and held for 12 hours and quenched to room temperature in approximately 20 min. Specimens 6, 7, and 8A were not run concurrently with the others but were subjected to the same heat treating schedule. The B series experiments were raised to 2156°C for 15 minutes, quenched in He to 1545°C, held for 12 hours and quenched to room temperature in approximately 20 minutes.

X-ray diffraction analysis was performed on both series, Table VI

Table V. Interfacial and Liquid Zone Compositions of Mullite in Diffusion Couple Experiments.*

Specimen Designation	Temp °C	Weight Percentage Oxides					
		Mullite Layer			Mullite Precipitates		
		CaO	Al_2O_3	SiO_2	CaO	Al_2O_3	SiO_2
4.01.74B	1707	<0.1	75.7	24.2	<0.1	76.2	23.8
4.03.74B	1707	<0.1	78.2	21.7	<0.1	77.8	22.1
5.01.74B	1707	<0.1	77.0	22.9	<0.1	77.3	22.6
4.03.74C	1602	<0.1	75.2	24.7	<0.1	76.3	23.6
5.01.74C	1602	<0.1	76.4	23.5	<0.1	76.7	23.2

*The A series is not included here because the sapphire was entirely dissolved and no values could be obtained at the interface.

Table VI. Summary of X-ray Data on Quenched Specimens: Mullite Lattice Parameters

Sample Designation	Lattice Parameters a_o	b_o	c_o	V_C*	Phases Detected
1A	7.561	7.686	2.890	167.940	Mullite
2A	7.559	7.683	2.892	167.985	Mullite
3A	7.561	7.684	2.897	168.312	Mullite
4A	7.573	7.687	2.899	168.587	Mullite
6A	7.561	7.686	2.891	168.018	Mullite & α-Alumina
7A	7.563	7.687	2.888	167.835	Mullite & α-Alumina
5A	7.567	7.676	2.885	167.760	Mullite & α-Alumina
8A	7.562	7.687	2.887	167.822	Mullite & α-Alumina
1B	7.556	7.688	2.885	167.579	Mullite
2B	7.557	7.684	2.890	167.794	Mullite
3B	7.561	7.685	2.890	167.927	Mullite
4B	7.570	7.680	2.895	168.318	Mullite
5B	7.575	7.678	2.885	167.774	Mullite & α-Alumina

*Any multiplication discrepancies between the axes parameters and the unit cell volume are the result of rounding of the computer output. See Appendix II.

0 0 1 8 4 6 9 7 3 8 7

but only the A series was subjected to electron beam microprobe analysis, Table VII. No attempt was made at accurate lattice parameter identification as only changes in values were needed. In previous X-ray studies, ordered and disordered mullite had been discussed by a number of investigators including Agrell and Smith.[43] They saw a distinction between sharp and diffuse mullite where diffuse mullite was attained by quenching of aluminum-silicate melts. The order-disorder transition in mullite must therefore explain the variations in lattice parameter values observed when heat treatments and alumina content are varied. Kramer[44] did an extensive review covering mullite X-ray data and procedures and noted the general disagreement among authors as to which indicators are most sensitive to the mullitization process. This present study is in agreement with Majumdar and Welch[45] who noted that the a_o and c_o dimensions of the orthorhomic unit cell increase while b_o was unaffected due to increasing alumina content. Roy[2] observed a greater increase in the a_o parameter than that of c_o for a given increase in the alumina content from 3:2 type to 2:1 type mullite while Majumdar[45], Crofts[46], Tromel[47] and Gelsdorf[48] all agreed that a_o behaved linearly with respect to alumina content, but only for mullite precipitated from the melt. Figures 9 and 10 depict the variation in the a_o and c_o parameters versus the wt% Al_2O_3 in the mullite crystals. The decrease in a_o and c_o values for specimens 6A, 7A and 8A, where α-Al_2O_3 has precipitated as a second phase, probably indicates that these parameters are sensitive to composition and show a direct dependence on Al_2O_3 content with the more striking reduction in value at the upper limit of the 2:1 type mullite solid solution range.

Table VII. Crystal-Matrix Compositions* of Quenched Specimens in the Binary Al_2O_3-SiO_2 System.

Specimen Designation	Compositions in wt% Oxides — Initial Melt		Mullite Crystal		Liquid		Crystal Phase #
	Al_2O_3	SiO_2	Al_2O_3	SiO_2	Al_2O_3	SiO_2	
1A	65.0	35.0	71.7	28.3	37.1	62.9	Mullite
2A	70.0	30.0	72.6	27.4	21.0	79.0	Mullite
3A	75.0	25.0	79.3	20.7	20.0	80.0	Mullite
4A	80.0	20.0	82.7	17.3	No Liquid Phase		Mullite
6A	82.5	18.5	78.9	21.1	No Liquid Phase		Mullite & α-Al_2O_3
7A	84.0	16.0	74.0	26.0	No Liquid Phase		Mullite & α-Al_2O_3
5A	85.0	15.0	+				Mullite & α-Al_2O_3
8A	87.5	12.5	79.0	21.0	No Liquid Phase		Mullite & α-Al_2O_3

*Average of 4 different readings

#By X-ray diffraction

+Crystal and/or liquid phase to small for reasonable microprobe determination.

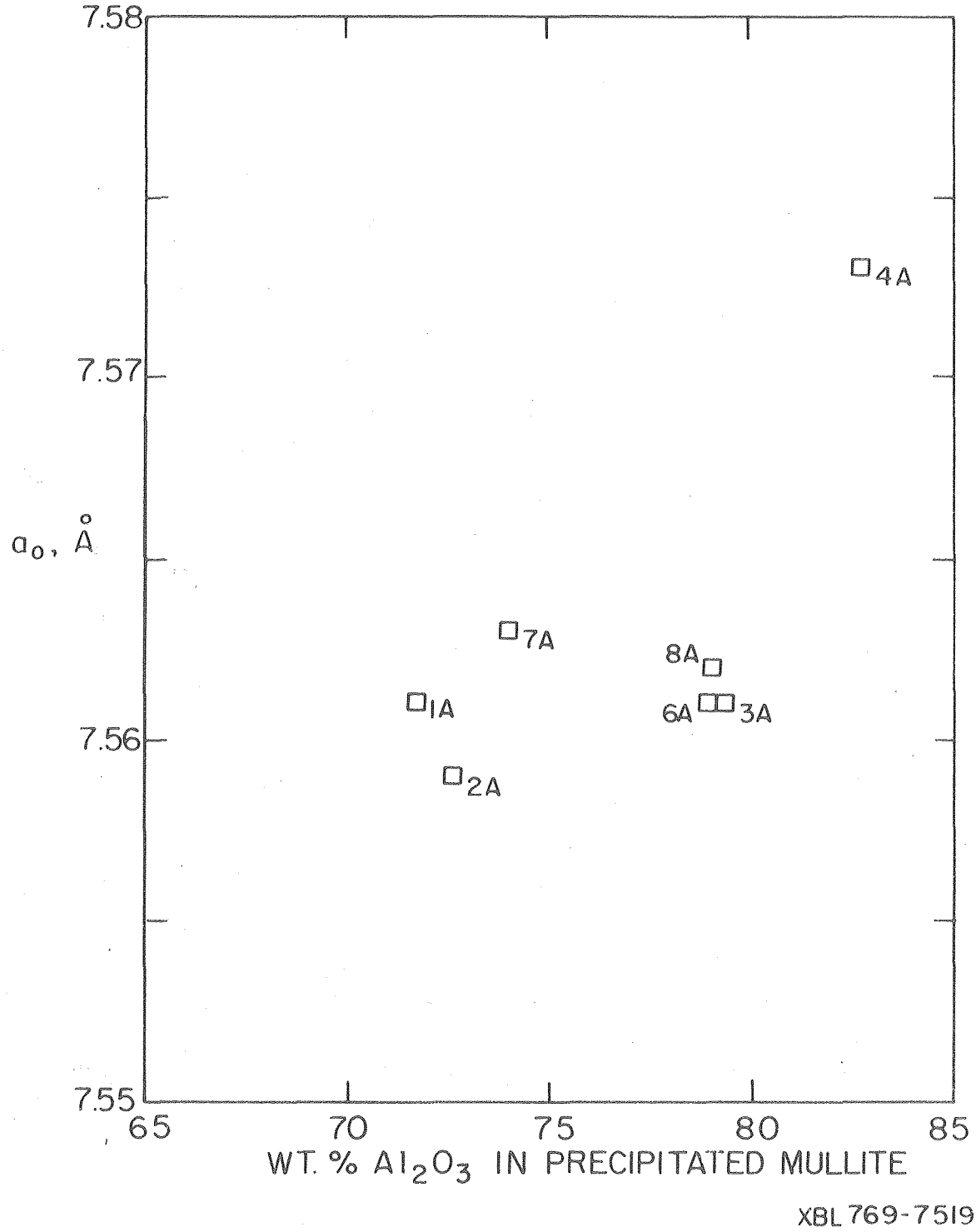

Fig. 9. a_o axis lattice parameter of mullites in quenched binary specimens versus the wt% Al_2O_3 in each.

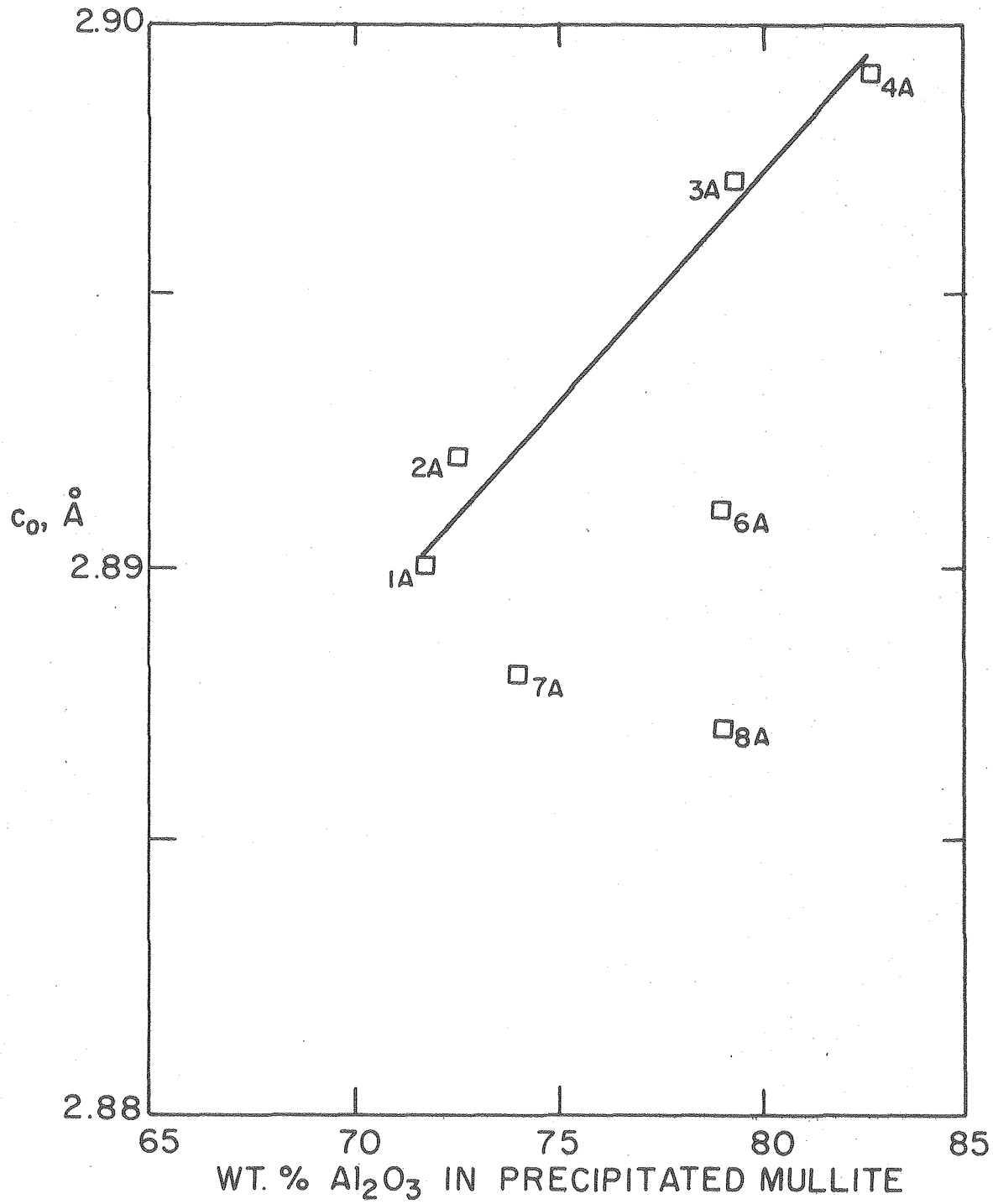

XBL 769-7520

Fig. 10. c_o axis lattice parameter of mullites in quenched binary specimens versus the wt% Al_2O_3 in each.

Agrell and Smith[43] also observed a linear relationship between unit cell volume, Vc, and c_o for Iron-free mullite. Figure 11 reinforces this observation up to the 2:1 type mullite solid solution limit. As the limit is exceeded with specimens 5A, 6A, 7A and 8A, and α-Al_2O_3 is now precipitating as a second phase, the unit cell volume decreases back to a value somewhat similar to that of stoichiometric 3:2 type mullite. This decrease is an expected result and confirms the 2:1 type mullite solid solution limit of Aksay and Pask, i.e., as the upper limit of this solution range is passed the system should and does revert to the stable binary Al_2O_3- SiO_2 diagram, Fig. 2. Microprobe data listed in Table VII and microstructures in Figs. 12, 13 and 14 reaffirm this observation.

Specimens higher than ≈82.5 wt% Al_2O_3 demonstrate a two-phase microstructure consisting of mullite and α-Al_2O_3 while those below this limit show the mullite composition increasing in Al_2O_3 content up to 80 wt% Al_2O_3 and then showing an expected drop back towards the 3:2 type mullite composition solid solution range.

Although the X-ray data from specimen 5A is consistent with its counterparts, the observed microstructure does not conform to that expected. No mullite crystals were found large enough for electron beam microprobe analysis. Consequently, the data point is omitted in Figs. 9 and 10.

The B series was not subjected to any electron beam microprobe analysis and was therefore not included in the depicted results. The c_o parameter followed the same path as that for the A series and decreased in value at approximately the same melt composition.

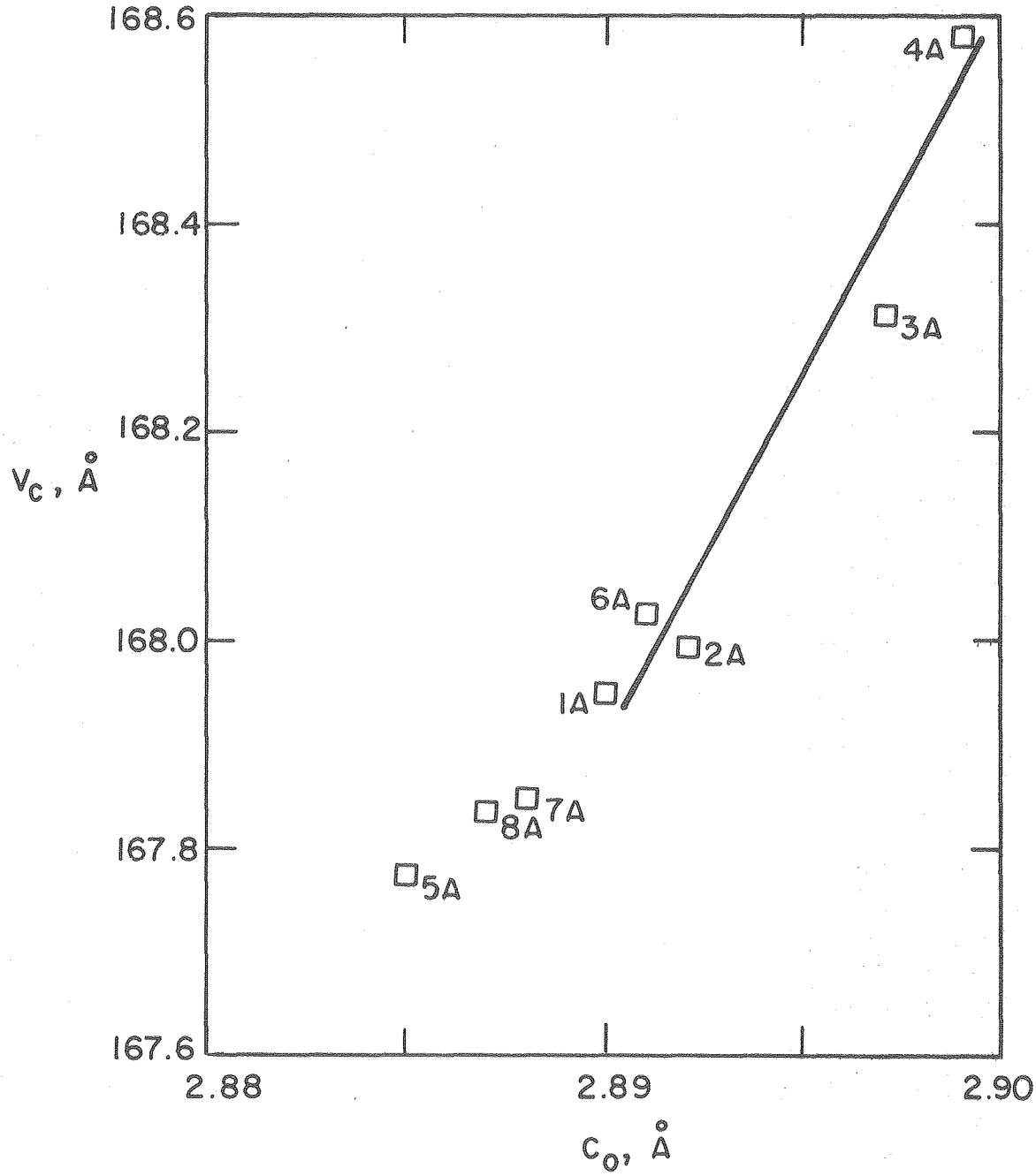

XBL769-7521

Fig. 11. Unit cell volume of mullites in quenched binary specimens versus their C_o axis parameter.

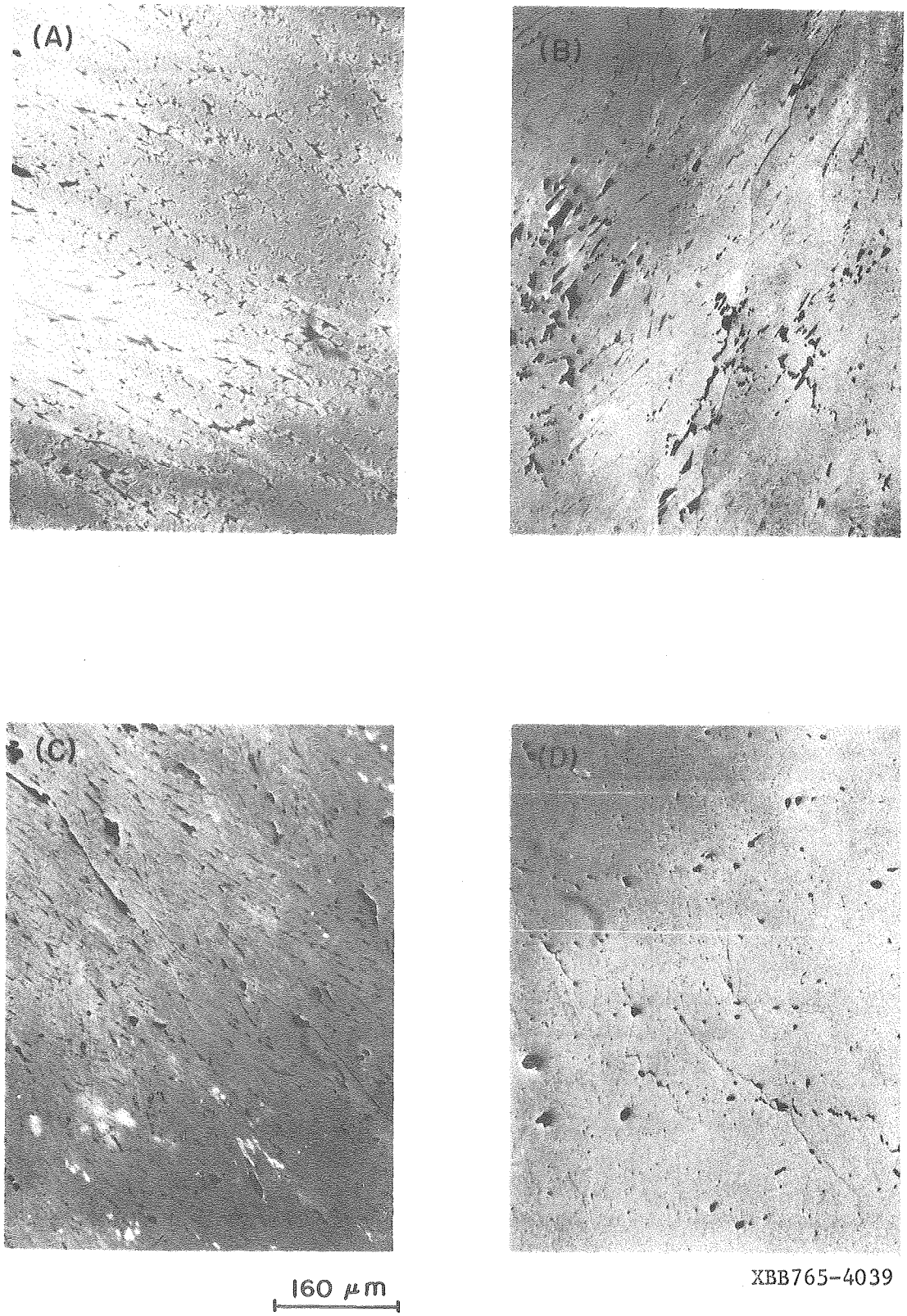

Fig. 12. Interference-contrast micrographs of quenched binary Al_2O_3-SiO_2 specimens 1A, 2A, 3A and 4A after a 12 hour hold at 1804°C. a) 65 wt% Al_2O_3, b) 70 wt% Al_2O_3, c) 75 wt% Al_2O_3, d) 80 wt% Al_2O_3.

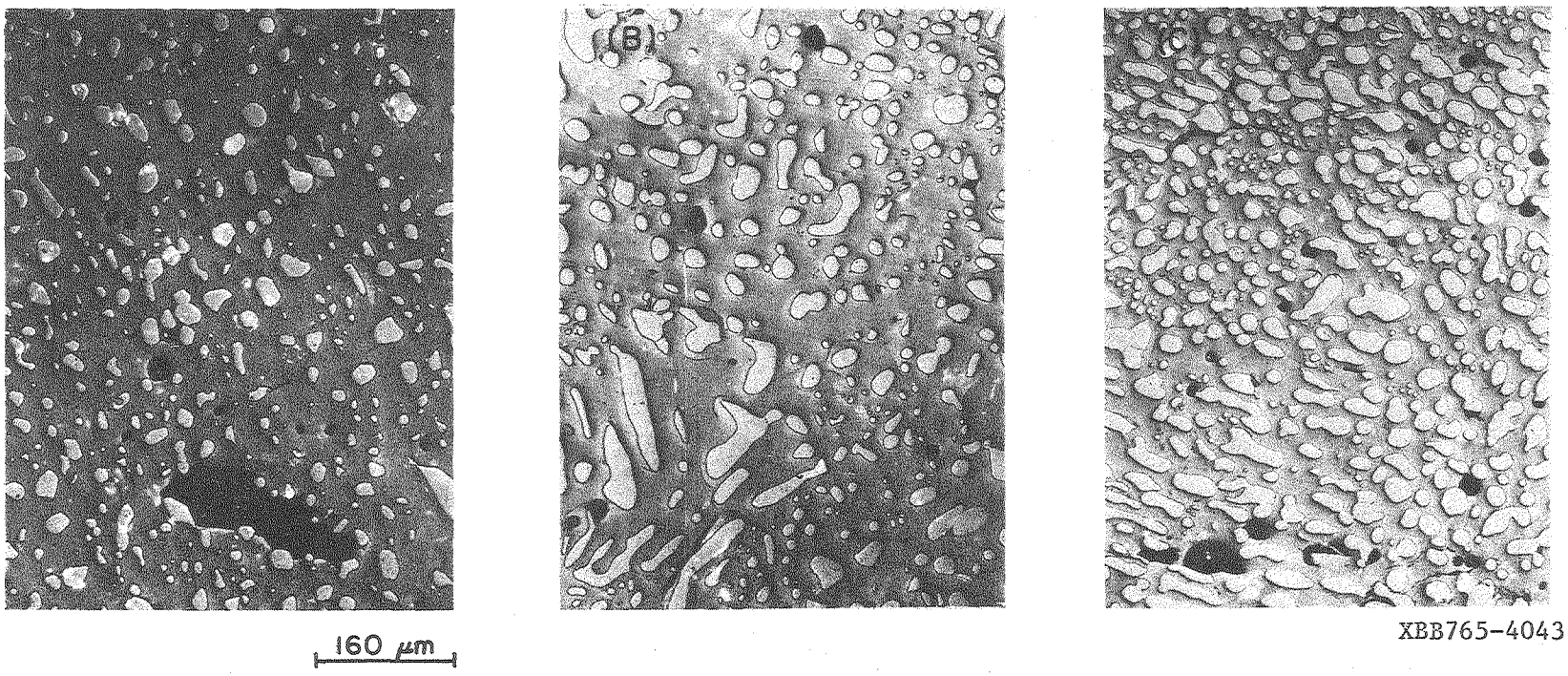

XBB765-4043

Fig. 13. Interference-contrast micrographs of quenched binary Al_2O_3-SiO_2 specimens 6A, 7A, and 8A after a 12 hour hold at 1804°C. a) 82.5 wt% Al_2O_3, b) 84. wt% Al_2O_3, c) 87.5 wt% Al_2O_3.

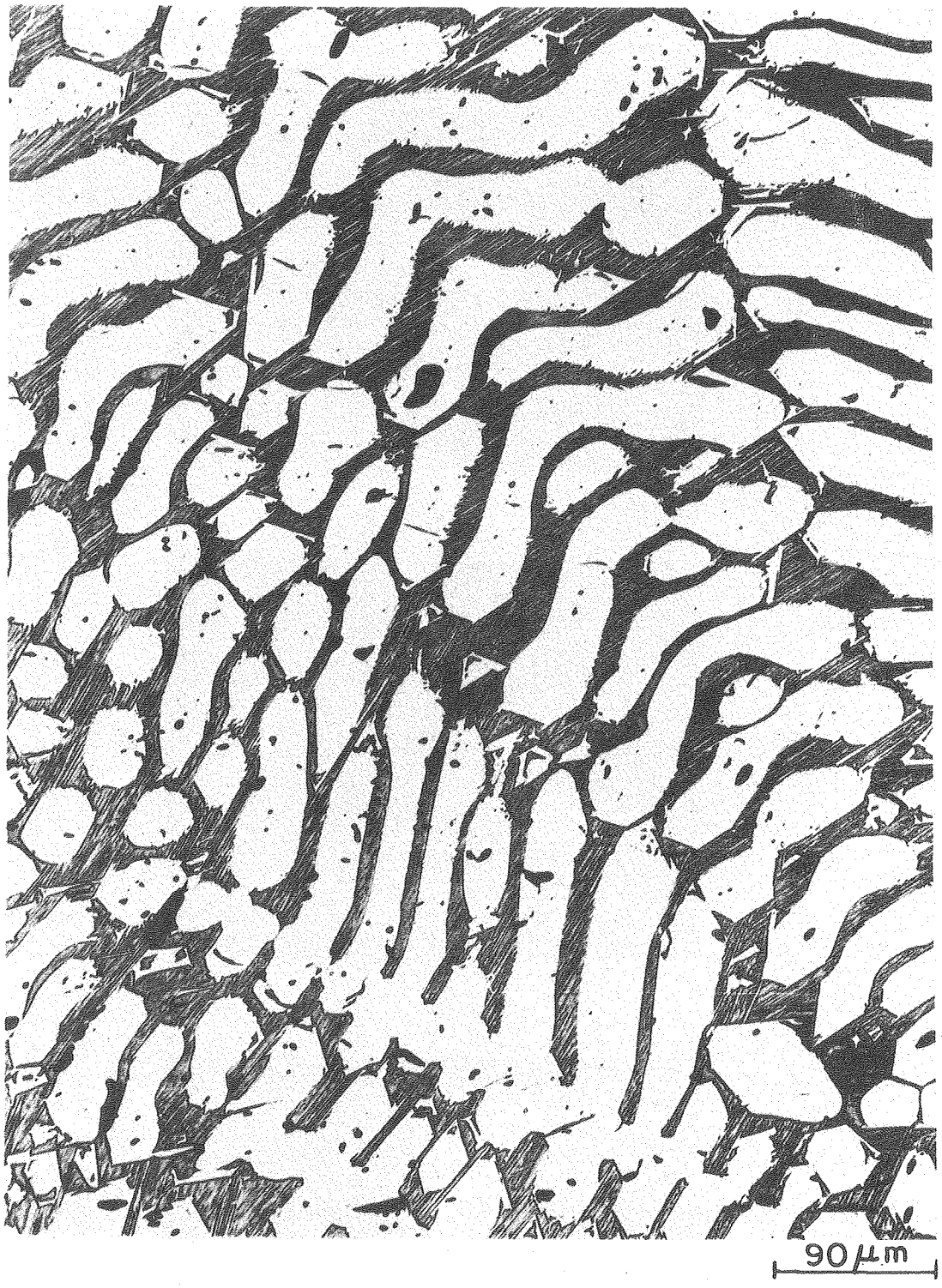

Fig. 14. Interference-contrast micrograph of quenched binary Al_2O_3-SiO_2 specimen 5A after a 12 hour hold at 1804°C 85 wt% Al_2O_3.

2. Mullite Solid Solution in the $CaO-Al_2O_3-SiO_2$ System

Two series of experiments, each containing 7 specimens, were conducted in an attempt to establish the solid solubility limits of CaO in mullite and to establish any further evidence towards metastability in this system and to duplicate some of the ternary experiments of Aramaki and Roy.[2] Each composition is listed in Table III.

The 9.XX.75 series was homogenized at 2150°C for 1 hour, quenched to 1807°C, held for 12 hours and quenched to room temperature in ≈20 minutes. Series 11.13.75X did not follow a regular pattern in composition as the 9.XX.75 series. The purpose here was to bracket both of the proposed mullite-corundum phase boundaries in order to provide information for determining phase boundaries. The compositions in this series closely approximate those used by Aramaki and Roy.[2] Instead of an immediate quench, however, the specimens were homogenized at 2162°C and slowly cooled from this temperature to 1400°C in 6.8 days (4.5°C/hr.) and then quenched to room temperature in approximately 20 minutes.

After heat treatment each specimen was sectioned, polished as described in Section III-A, and subjected to X-ray diffraction analysis, when mullite was present, and microprobe analysis.

X-ray diffraction analysis results of the 9.XX.75 and 11.13.75X series are listed in Table VIII.

Prior to electron beam microprobing of the polished 9.XX.75 specimens, it was necessary to obtain some information about the CaO distribution throughout the samples. To accomplish this, X-ray density maps, Fig. 15, were obtained over an area of approximately 300μm x 400μm. It was indicated from these density maps that CaO solubility

Table VIII. Summary of X-ray Data on Quenched Ternary Specimens; Mullite Lattice Parameters.

Sample Designation	Lattice Parameters a_o	b_o	c_o	V_c	Phases Detected
9.01.75	7.562	7.688	2.891	168.064	Mullite
9.02.75	7.564	7.686	2.894	168.223	Mullite
9.03.75	7.565	7.686	2.895	168.343	Mullite
9.04.75	7.565	7.686	2.899	168.551	Mullite
9.05.75	No Mullite Detected				α-Al_2O_3
9.06.75	No Mullite Detected				α-Al_2O_3
9.07.75	No Mullite Detected				α-Al_2O_3
11.13.75A	*				Mullite
11.13.75B	No Mullite Detected				α-Al_2O_3
11.13.75C	No Mullite Detected				Amorphous
11.13.75D	7.562	7.685	2.886	167.715	Mullite
11.13.75E	No Mullite Detected				α-Al_2O_3
11.13.75F	7.568	7.683	2.889	168.016	Mullite & α-Al_2O_3
11.13.75G	No Mullite Detected				α-Al_2O_3

*Insufficient Amount of Mullite Crystals for Accurate Lattice Parameter Measurements.

0 0 0 4 6 0 7 5 9 3

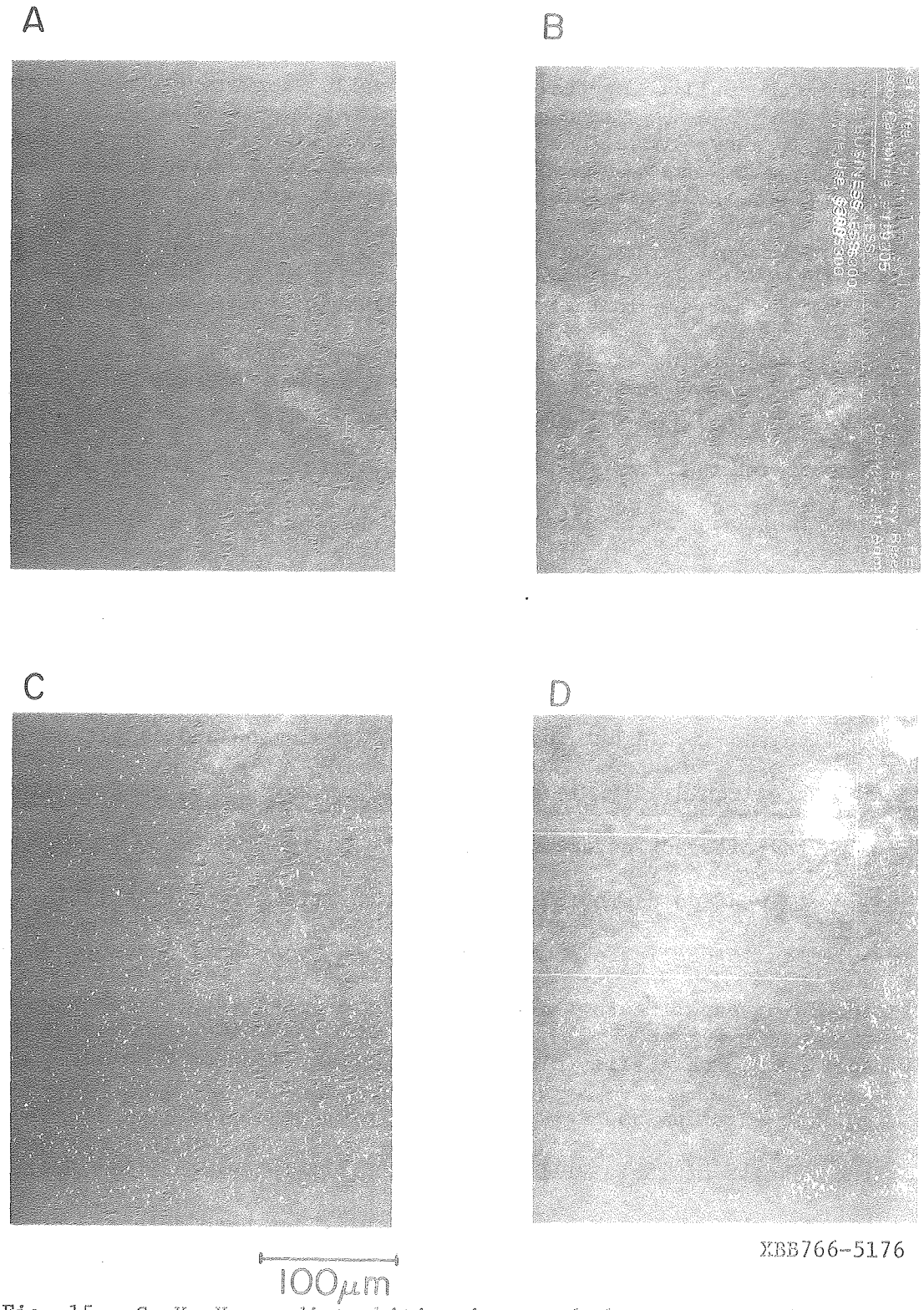

XBB766-5176

Fig. 15. Ca K_α X-ray distrubition in quenched ternary specimens. a) 9.01.75: No CaO, b) 9.02.75: 2 wt% CaO, c) 9.03.75: 5 wt% CaO, d) 9.04.75: 10 wt% CaO.

within the mullite crystal was very small. Pockets of Ca concentration begin to show almost immediately and grow with increasing CaO content.

After the compositions of the crystals and matrix were obtained from the electron beam microprobe, Table IX, it was evident from the results that the increase in the unit cell volume of the mullite crystals was due to increasing alumina content and not to any solid solubility of CaO. Figure 16 represents this increase in unit cell volume vs. alumina content of the mullite crystals. The CaO present in each specimen now constitutes an ever increasing liquid phase, Fig. 17, that is increasingly richer in CaO.

At a composition where the CaO has reached 12.5 wt% in the melt, for the 9.XX.75 series, the corresponding microstructure is no longer that of mullite and liquid but instead that of α-alumina and a calcium-aluminum silicate liquid, Fig. 18. At no time was any anorthite detected, either by X-ray diffraction or in composition by electron beam microprobe.

As mentioned previously, the compositions in series 11.13.75X were selected to duplicate some of those used by Aramaki and Roy[2] in their quenching experiments. X-ray diffraction results of these slow cooled specimens, Table VIII, clearly indicate a different location of the mullite-corundum boundary than their proposed boundary. If one compares the results of Table VIII with Fig. 20, it is evident that had the old boundary been correct, no alumina should have been detected for the 11.13.75F composition.

The results of the electron beam microprobe on the crystal matrix compositions are shown in Table IX. Optical micrographs of each

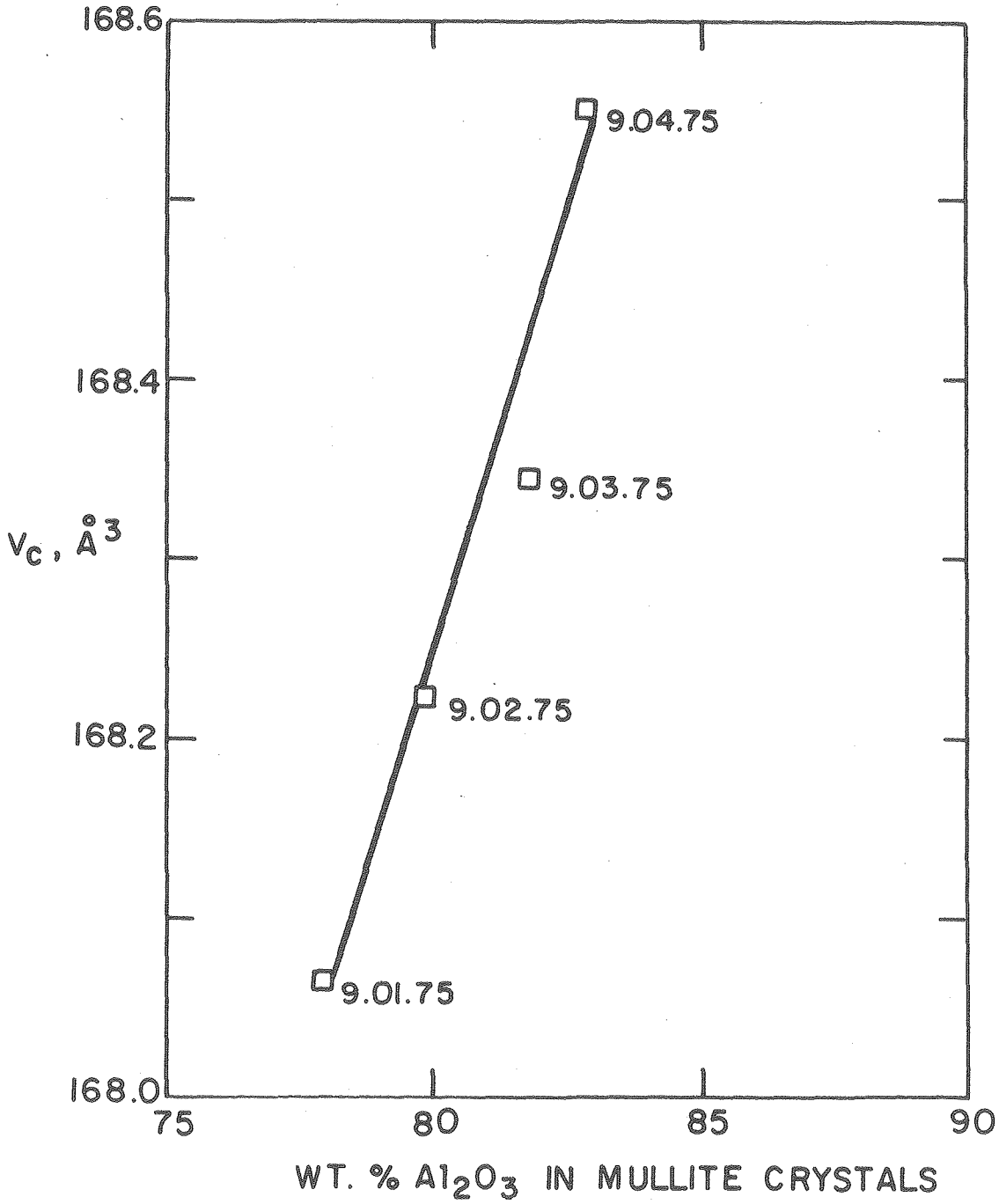

XBL 769-7518

Fig. 16. Unit cell volume of mullites in quenched ternary specimens as a function of their Al_2O_3 wt%.

Table IX. Crystal-Matrix Compositions[Δ] for Quenched Specimens in the Ternary $CaO-Al_2O_3-SiO_2$ System.

Specimen Designation	Temp °C	Compositions in Wt% Oxides: Initial Melt CaO	Initial Melt Al_2O_3	Initial Melt SiO_2	Mullite Crystal CaO	Mullite Crystal Al_2O_3	Mullite Crystal SiO_2	Liquid CaO	Liquid Al_2O_3	Liquid SiO_2	Phases Detected[#]
9.01.75	1817	-	71.79	28.21	-	77.9	22.1	-	59.0	41.0	Mullite
9.02.75	1817	2.00	70.35	27.65	0.9	79.8	19.3	10.0	45.0	45.0	Mullite
9.03.75	1817	5.00	68.20	26.80	0.4	81.7	17.9	19.1	33.8	47.1	Mullite
9.04.75	1817	10.00	64.61	25.39	0.3	82.8	16.9	20.3	30.9	48.8	Mullite
9.05.75	1817	12.50	62.82	24.68	-	100.0	-	17.7	43.5	38.8	$\alpha-Al_2O_3$
9.06.75	1817	15.00	61.02	23.98	-	100.0	-	14.8	30.0	55.2	$\alpha-Al_2O_3$
9.07.75	1817	20.00	57.43	22.57	-	100.0	-	+			$\alpha-Al_2O_3$
11.13.75A	*	10.09	29.75	60.16	0.9	77.2	21.9	36.7	20.0	43.3	Mullite
11.13.75B	*	19.93	40.00	40.07	-	100.0	-	27.7	32.4	39.9	$\alpha-Al_2O_3$
11.13.75C	*	9.99	39.90	50.10	-	-	-	10.6	37.3	52.1	Amorphous
11.13.75D	*	4.91	44.88	50.21	0.8	76.7	22.5	21.3	24.8	53.9	Mullite
11.13.75E	*	9.93	49.98	40.09	-	100.0	-	20.5	29.0	50.5	$\alpha-Al_2O_3$
11.13.75F	*	5.08	54.99	39.93	0.5	81.5	18.0	8.0	56.9	35.1	Mullite & $\alpha-Al_2O_3$

Continued Next Page

Table IX. (Continued)

Specimen Designation	Temp °C	Compositions in Wt% Oxides: Initial Melt CaO	Initial Melt Al_2O_3	Initial Melt SiO_2	Mullite Crystal CaO	Mullite Crystal Al_2O_3	Mullite Crystal SiO_2	Liquid CaO	Liquid Al_2O_3	Liquid SiO_2	Phases Detected#
11.13.75G	*	9.98	59.56	30.46	-	100.0	-	33.8	31.2	35.0	α-Al_2O_3

Δ Averaged values for 4 areas

By X-ray Diffraction

+ Phase distribution did not lend itself to microprobe determination.

* Instead of an immediate quench, this series was cooled from 2150°C to 1400°C at a rate of 4.5°C per hour (6.8 days).

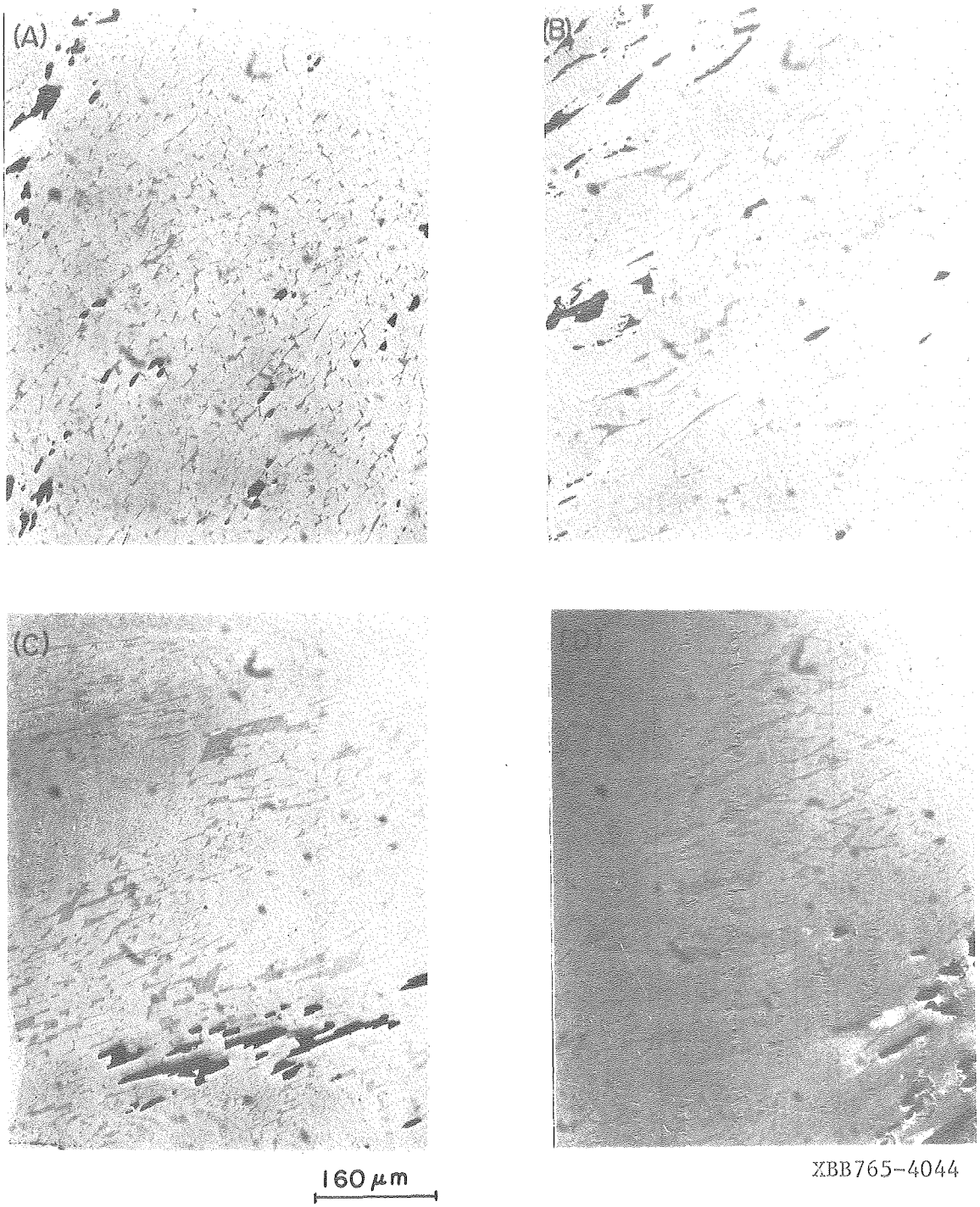

XBB765-4044

Fig. 17 Interference-contrast micrographs of quenched ternary $CaO-Al_2O_3-SiO_2$ specimens 9.01.75, 9.02.75, 9.03.75 and 9.04.75 after a 12 hour hold at 1817°C. a) 3:2 mullite, b) 3:2 mullite + 2 wt% CaO, c) 3:2 mullite + 5 wt% CaO. d) 3:2 mullite + 10 wt% CaO.

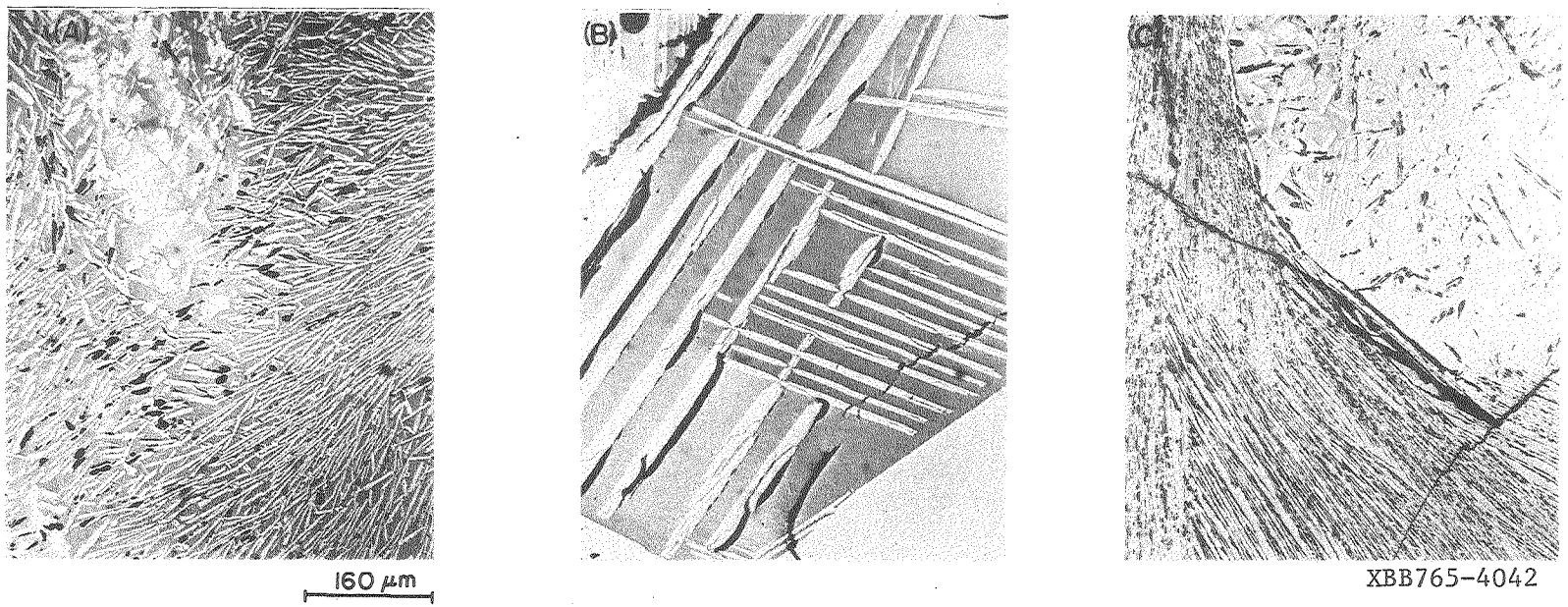

Fig. 18. Interference-contrast micrographs of quenched ternary $CaO-Al_2O_3-SiO_2$ specimens 9.05.75, 9.06.75, and 9.07.75 after a 12 hour hold at 1817°C. a) 3:2 mullite + 12.5 wt% CaO, b) 3:2 mullite + 15 wt% CaO, c) 3:2 mullite + 20 wt% CaO.

specimen are depicted in Fig. 19. Specimen 11.13.75C is not shown as the crucible integrity was lost during the heat treatment and the resulting microstructure and X-ray analysis showed the sample to be amorphous.

D. Stable and Metastable Mullite Phase Equilibria

Figures 20 and 21 are partial representations of the $CaO-Al_2O_3-SiO_2$ ternary system as it has been updated by this author. The main differences between these and the currently accepted diagram, Fig. 3, by Osborn and Muan[49] are (1) the establishment and revision of the calcium hexaluminate ($CaO.6Al_2O_3$) stable phase field by Gentile and Foster[50], (2) the updating and establishment of isotherm locations using the data of this author, Aksay and Pask[3] and Gentile and Foster and the new mullite-corundum boundary. Now, had the binary revision by Aramaki et al.[1] been correct, we should naturally expect a ternary diagram showing mullite as a congruently melting compound, Fig. 3, but since recent studies have conclusively demonstrated mullite's incongruency the currently excepted ternary diagram was expected to be in error. Figure 20 depicts the proposed location of this mullite-corundum boundary, which is quite similar to that proposed by Grieg[34] as would be consistent with an incongruently melting compound. The possibility exists, however, that because of the metastable tendencies of the alumina-silica system and its only compound, mullite, that the current phase diagram in the mullite region, Fig. 3, actually is only representative of a metastable condition. The quenching experiments with the ternary compositions, Table III, were conducted with the intention of determining the extention of the metastable phase field of mullite into the interior portion of the ternary diagram.

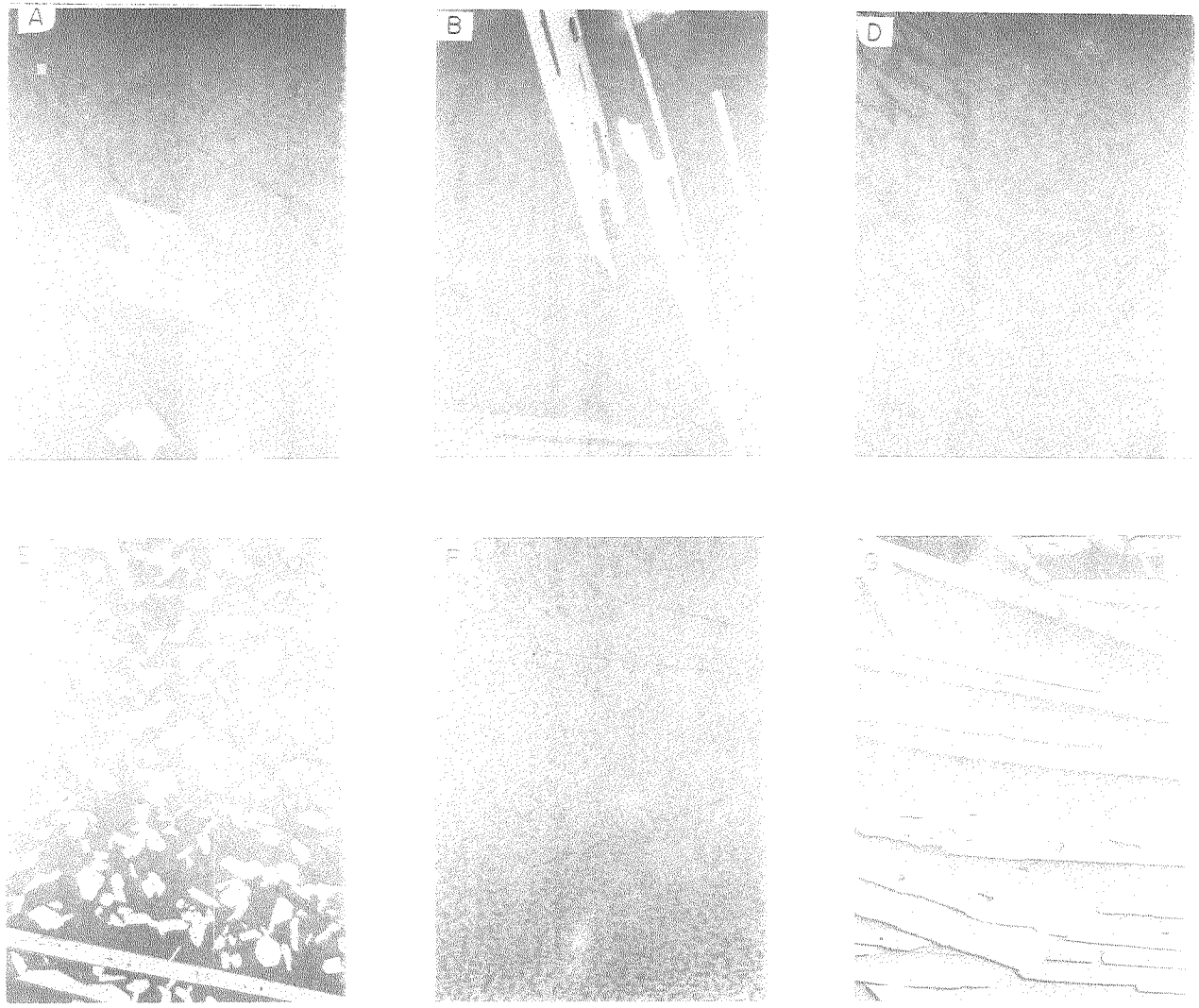

Fig. 19. Interference contrast micrographs of slow cooled ternary CaO-Al O -SiO specimens 11.13.75A→G. Specimen C is not included due to its lack of microstructure. See Table IX for compositions and crystal phases.

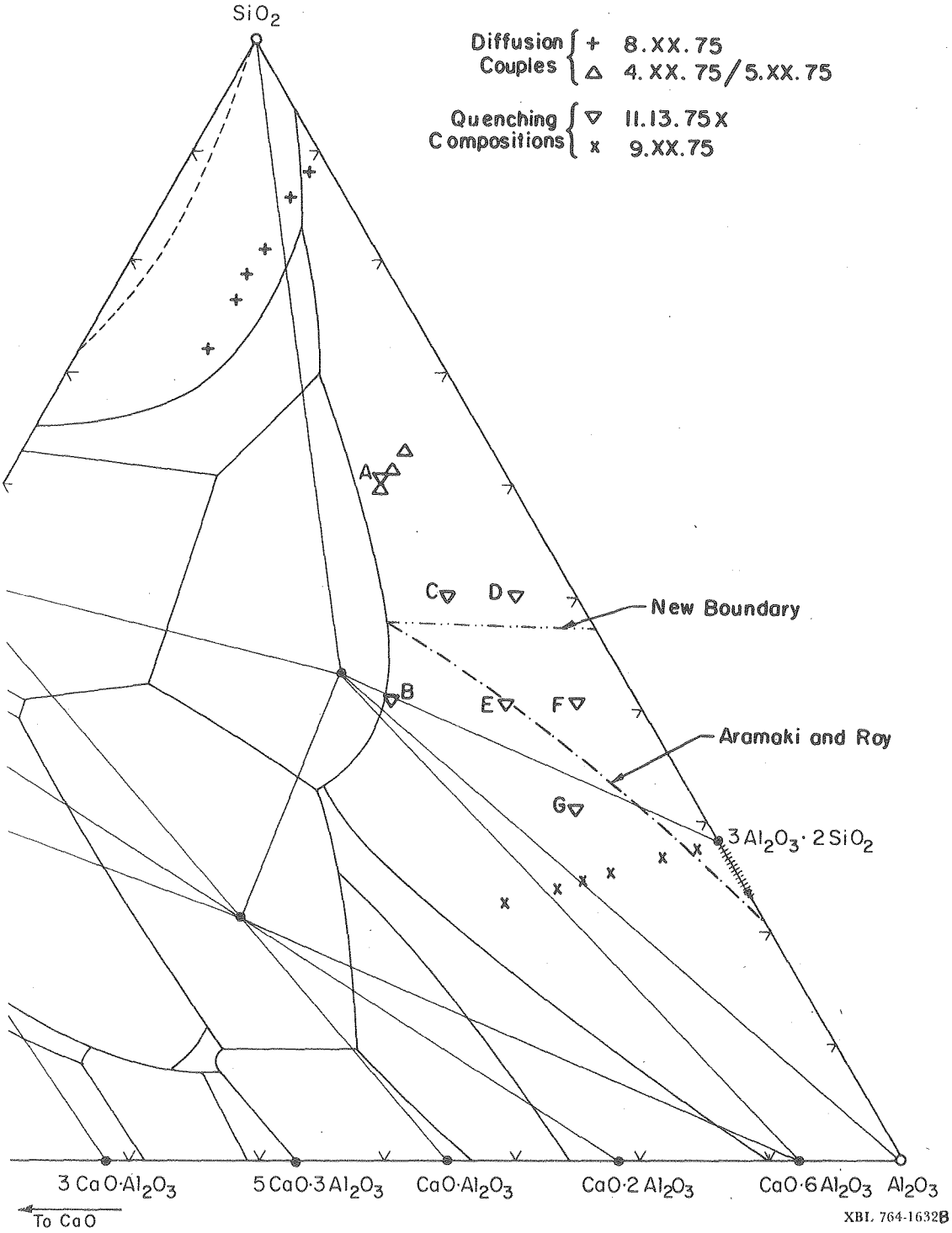

Fig. 20. Revised $CaO-Al_2O_3-SiO_2$ ternary phase diagram showing location of the mullite-corundum boundary as proposed by Aramaki and Roy[2] and this author. Initial composition points of diffusion couple liquids and quenching experiments are also shown. See Tables I and III for actual compositions.

0 0 0 0 4 6 0 7 5 9 8

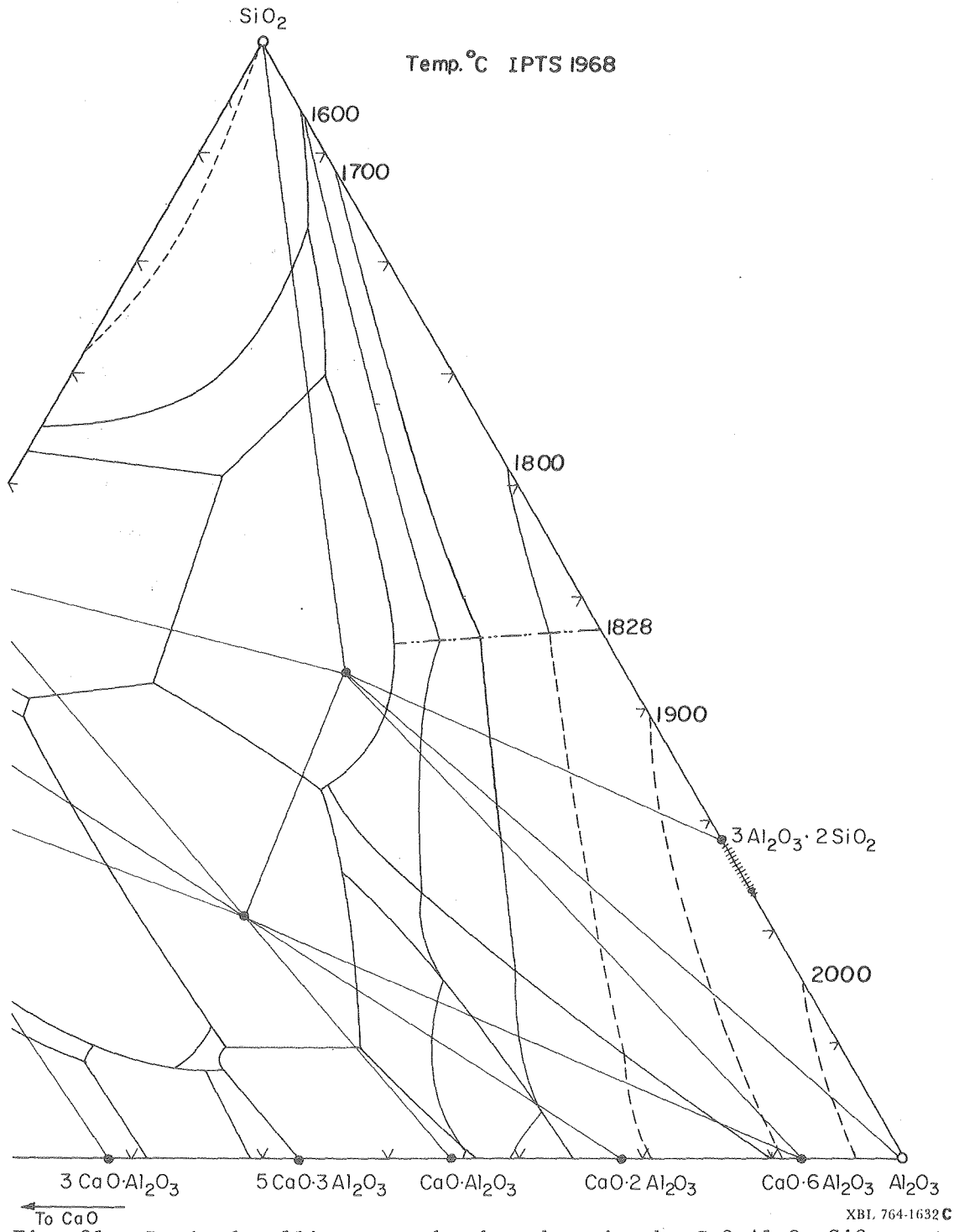

Fig. 21. Revised mullite-corundum boundary in the $CaO-Al_2O_3-SiO_2$ system showing established isotherms for the mullite primary phase field and estimated isotherms for the corundum, calcium hexaluminate and calcium dialuminate phase fields.

Microprobe results of the actual crystal and liquid compositions, Table IX, and microstructures of these melts, Figs. 17, 18 and 19, do not allow extention of any metastable boundary into the ternary interior by more than ~1 wt% CaO. This 1 wt% CaO in the quenching experiments is consistent with the electron beam microprobe determination obtained in the diffusion experiments, Table V, which shows less than 0.1 wt% CaO.

From the diffusion couple experiments, accurate positioning of the isotherms in the mullite phase field was possible. This was accomplished from knowledge of the temperature of the individual experimental runs and determining the average interfacial compositions over an ≈40 μm scan at the sapphire-liquid interface.

0 0 0 0 4 6 0 7 5 9 9

V. DISCUSSION AND CONCLUSION

A. CaO Effects on Mullite Phase Equilibria

1. Diffusion Experiments

The inability to realize any stable 3:2 type mullite layer at the sapphire-liquid interface hampered attempts to establish the proper location of the mullite-corundum boundary. The fact that only the 2:1 type composition or higher was detected is clear evidence that the mullite present both as a layer at the interface and in the liquid portion of the diffusion couple precipitated from the melt.

As mentioned previously, one of the main criterion for the diffusion couple technique to be effective is to have the reaction sequences proceed under diffusion control. It may be possible that with the addition of CaO into the liquid phase, viscosity is reduced to the point where reactions are no longer diffusion controlled. One would still expect a stable growth layer of 3:2 type mullite but of molecular scale. If the liquid had not been saturated with Al_2O_3 dissolution of this layer at its interface would therefore proceed much faster than any diffusion process and thus produce no effective growing mullite layer. On the basis of the binary revision by Aksay and the pseudo-binaries constructed for this study, 30 wt% Al_2O_3 liquids at the temperatures used should have been adequate for Al_2O_3 saturation of the melt. One can only surmise that with the addition of CaO the solubility limit necessary for diffusional growth of mullite is much higher than that used or viscosity effects are predominate as mentioned above.

Although the ternary quenching experiments in this study which were slow cooled do confirm the existence of a different boundary, one that is more in line with the incongruent melting behavior of mullite, the diffusion results have been inconclusive and may be an indication of some definite limitations of the diffusion couple technique.

In view of the very limited CaO solid solubility (<0.1 wt%) detected within the mullite crystals in these diffusion runs, it may be possible that in the presence of any excess CaO beyond its solubility limit there is a tendancy to shift any stable phase equilibria towards the metastable. This was somewhat evident in the ternary quenching experiments where we see metastable mullite appearing in melts with compositions as high as 10 wt% CaO and lying well within the corundum primary phase field and may well account for never detecting any 3:2 mullite at the diffusion couple interfaces.

Positioning of isothermal lines in the mullite phase field was possible only for that portion of the field above the proposed boundary for an incongruent melting mullite. Lack of supporting evidence for the exact location of this boundary prevents extending these isotherms any further. Only estimates of their actual location can be made, Fig. 21.

2. Quenching Experiments

The solid solubility of CaO in mullite from the diffusion couple experiments was reported as being less than 0.1 wt%. Under quenching conditions, it is not uncommon for solubility to increase due to metastable extensions of stable phase boundaries. For these quenches, series 9.XX.75 and 11.13.75X, in the ternary system, the amount of CaO

present in any mullite crystal increased approximately an order of magnitude up to ≈1.0 wt%.

In addition to the increased solubility mullite is seen to exist metastably, under quenching conditions, up to a point between 10.0 wt% and 12.5 wt% CaO on a join between 3:2 mullite and CaO.

Results of the slow-cooled series, 11.13.75X, differ substantially from those obtained by Aramaki and Roy. This data reinforces the boundary as proposed in this study. Their short anneal times and the inability to liquify their samples to obtain homogeneous melts in all probability hampered any possibility of obtaining stable equilibria.

While not confirming its actual location, this series does establish the presence of the boundary at a point much closer to that expected from Aksay and Pask's binary Al_2O_3- SiO_2 studies.

B. <u>The Metastable Disordered Mullite Boundary for Binary Al_2O_3- SiO_2</u>.

The decrease in alumina content of the mullite crystals after crossing the metastable disordered solubility limit is a definite indication of that limits existence. Once the overall melt composition exceeded the ≈82.5 wt% Al_2O_3 limit, we see both a decrease in some unit cell values and Al_2O_3 content of the mullite. Figures 9 and 10 depicted the change in lattice parameter values with the mullites' alumina content. Figure 22 takes a slightly different approach and uses the precipitated crystal composition for the independent variable and the original melt composition as the dependent variable. This figure provides a more striking example of the change in mullite composition at the solubility limit.

The highest Al_2O_3 content detected for mullite in this study was

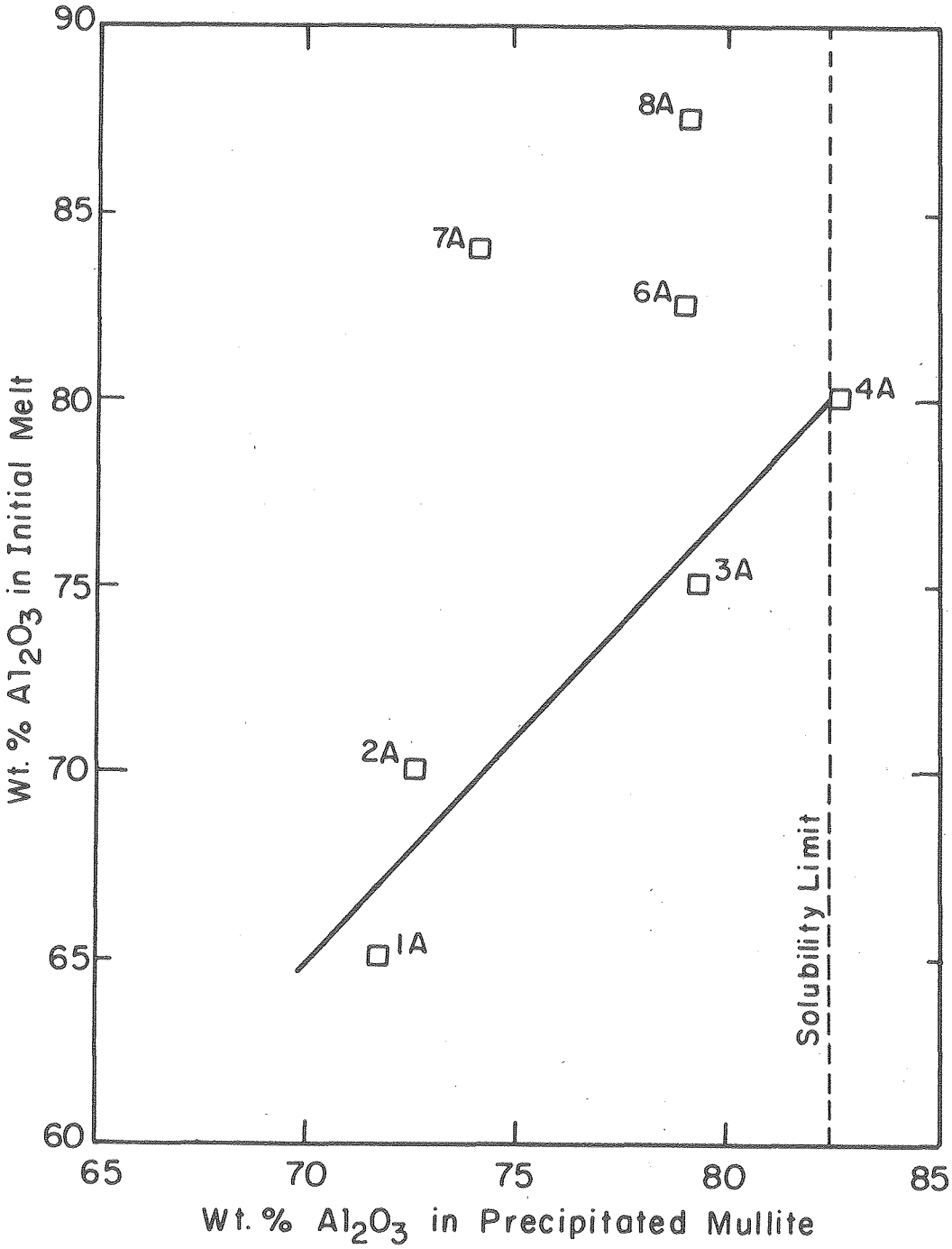

XBL 768-7337

Fig. 22. Representation of variation in Al_2O_3 content of mullite crystals vs. the initial melt content for binary Al_2O_3-SiO_2 quench specimens 1A→8A.

0 0 0 0 4 6 0 / 6 0 1

82.8 wt%. This value is in excellent agreement with previous authors and the lattice parameter values substantiate this as the upper solubility for the 2:1 type mullite.

ACKNOWLEDGMENT

I wish to express my appreciation to Professor Joseph A. Pask for his excellent guidance, encouragement and helpful criticism throughout this research. Colleagues and friends, in particular, Subash Risbud were always there with a helpful ear.

Professors Richard M. Fulrath and Leo Brewer critically read and commented on the manuscript.

Grateful acknowledgments are extended to the support staff of the Materials and Molecular Research Division of the Lawrence Berkeley Laboratory who assisted the project in numerous ways. Thanks are due Richard Lindberg (Electron Beam Microprobe assistance), Walter Toutolmin and Glenn Baum (Crucible Fabrication and Mechanical Support), Jack N. Wodei (Electronic Equipment), Lee R. Johnson (Metallograph Instruction), Gloria Pelatowski (Technical Drawing), Kelly Radmilovic and Gay Brazil (Manuscript Preparation).

I especially acknowledge the patience and encouragement of my wife, Gwendolyn, which have contributed to the completion of this work.

This work was done with support from the U.S. Energy Research and Development Administration. Any conclusions or opinions expressed in this report represent solely those of the author and not necessarily those of the Lawrence Berkeley Laboratory nor of the U.S. Energy Research and Development Administration.

REFERENCES

1. S. Aramaki and R. Roy, J. Am. Ceramic Soc. 45 [5], 229-42 (1962).
2. S. Aramaki and R. Roy, J. Am. Ceramic Soc. 42 [12], 644-45 (1959).
3. I. A. Aksay and J. A. Pask, J. Am. Ceramic Soc. 58 [11-12], 507-12 (1975).
4. I. A. Aksay and J. A. Pask, "Determination of Phase Diagrams Using Diffusion Techniques", Mass Transport Phenomena in Ceramics, Edited by A. R. Cooper and A. H. Heuer, Plenum Publishing Corporation, (1975).
5. G. V. Kidson, Some Aspects of the Growth of Diffusion Layers in Binary Systems, J. Nucl. Mater. 3, 21-29 (1961).
6. G. B. Gibbs, Diffusion Layer Growth in a Binary System, J. Nucl. Mater. 20, 303-306 (1966).
7. F. N. Rhines, "Phase Diagrams in Metallurgy, Their Development and Application", pp. 50-52, 107-109, and 156-57, McGraw-Hill Book Co., New York (1956).
8. N. L. Bowen and J. W. Greig, J. Am. Ceramic Soc. 7 [4], 238 (1924).
9. W. H. Bauer, I. Gordon and C. H. Moore, J. Am. Ceramic Soc. 33 [4], 140 (1950).
10. N. A. Toropov and F. Y. Galakhov, Doklady Akad. Nauk SSSR 78 [2], 299 (1951) (in Russian).
11. N. E. Filonenko and I. V. Lavrov, Doklady Akad. Nauk SSSR 89 [1], 141 (1953) (in Russian).
12. K. Konopicky, Bull. Fr. Ceram. Soc. [33], 3-6 (1956) (in French).
13. G. Trömel, L.-H. Obst, K. Konopicky, H. Bauer and I. Patzak, Ber. Dtsch. Keram. Ges. 34 [12], 397 (1957) (in German).

14. G. Trömel, The Physical Chemistry of Steel-Making, J. F. Elliott, ed. (MIT Press, New York, 1958).

15. J. H. Welch, Nature 186 [4724], 545 (1960).

16. J. H. Welch, Observations on Composition and Melting Behavior of Mullite, Trans. 7th Int. Ceramic Congress, London, 1960, p. 197.

17. K. Konopicky, Ber. Dtsch. Keram. Ges. 40 [5] 286 (1963) (in German).

18. H. R. Müller, Ber. Dtsch. Keram. Ges. 40 [5], 316 (1963) (in German).

19. T. Horibe and S. Kuwabara, Bull, Chem. Soc. Japan 40 [4], 972 (1967).

20. P. P. Budnikov, S. G. Tresvyatski and V. I. Kushakovski, Doklady Akad. Nauk SSSR 93 [2] 281, (1953) (in Russian).

21. F. Y. Galakhov, Bull. Fr. Ceramic Soc. [38], 11 (1958) (in French).

22. S. Aramaki and R. Roy, Nature 184 [4686], 631 (1959).

23. N. A. Toropov and F. Y. Galakhov, The Al_2O_3-SiO_2 System, Eksperiment V Tekhn, Mineralog. i Petrogr., po Materialam Soveshch., 7th Lvov, 1966, p. 3 (in Russian).

24. G. Rehfeld and H. E. Schwiete, Ber. Dtsch. Keram. Ges. 48 [6] 258 (1971) (in German).

25. J. B. Macchesney and P. E. Rosenberg, Phase Diagrams, Materials Science and Technology, A. M. Alper, ed. (Academic Press, New York, 1970) Vol. 1, p. 113.

26. N. L. Bowen, The Evolution of the Igneous Rocks (Dover Publications, Inc., New York, 1956) p. 25.

27. W. Eitel, Silicate Melt Equilibria (Rutgers University Press, New Jersey, 1951).

28. R. F. Davis and J. A. Pask, J. Am. Ceramic Society 55 [10], 525 (1972).

29. W. H. Bauer and I. Gordon, J. Am. Ceramic Society 34 [8], 250 (1951).

30. A. L. Day, E. S. Shepherd, and F. E. Wright, Am. J. Sci. (4th Series), 22 265-302 (1906).

31. J. H. Welch and W. Gutt, J. Am. Ceram. Soc., 42, 11-15 (1959).

32. N. L. Bowen and J. W. Greig, J. Am. Ceram. Soc., 7, 238-54 (1924); corrections, ibid., 410.

33. G. A. Rankin and F. E. Wright, Am. J. Sci. (4th Series), 39 1-70 (1915).

34. J. W. Greig, Am. J. Sci. (5th Series), 13, 1-44; 133-54 (1927).

35. F. D. Rossini, J. Chem. Thermodynamics 2, 447 (1970).

36. S. J. Schneider and C. L. McDaniel, J. Res. NBS 71A [4], 317 (1967).

37. R. Theisen, Quantitative Electron Microprobe Analysis (Springer-Verlag, Inc., New York, 1965).

38. K. F. J. Henrich, ed., Quantitative Electron Probe Microanalysis, NBS Special Publication 298, Superintendent of Documents, U.S. Government Printing Office, Washington, D.C., 1968.

39. J. V. Smith, J. Geology 73 [6], 830-31 (1965).

40. J. Z. Frazer, R. W. Fitzgerald and A. M. Reid, Computer Programs EMX and EMX2 for Electron Microprobe Data Processing, Scripps Institute of Oceanography, University of San Diego, La Jolla, CA.

41. J. W. Colby, MAGIC IV, Microprobe Analysis General Intensity Corrections Program, Bell Telephone Laboratories, Inc., August, 1971.

42. C. W. Burnham, "Lattice Constant Refinement", Carnegie Institute of Washington, Annual Report of the Director of the Geophysical

Laboratory, pp. 132-35 (1961-62).

43. S. O. Agrell and J. V. Smith, J. Am. Ceram. Soc. 43 [2], 69 (1960).

44. C. M. Kramer, "Experiments on the Crystallization of Mullite," M.S. Thesis, LBL-3908, June 1975.

45. A. J. Majumdar and J. H. Welch, Trans. Brit. Ceram. Soc. 62 603 (1963).

46. J. D. Crofts and W. W. Marshall, Trans. Brit. Ceram. Soc. 66, 121 (1967).

47. G. Tromel, K.-H. Obst, K. Konopicky, A. Bauer and I. Patzak, Ber. Deut. Keram. Ges. 35, 108 (1958).

48. G. Gelsdorf, H. Müller-Hesse and H.-E Schweite, Arch. Eisenhuttenw. 29 [8], 513 (1958); Ceram. Abs., Sept. 1959, 236e.

49. E. F. Osborn and Arnulf Muan, revised and redrawn, "Phase Equilibrium Diagrams of Oxide Systems," Plate 1, published by the American Ceramic Society and the Edward Orton, Jr., Ceramic Foundation, 1960.

50. A. L. Gentile and W. R. Foster, J. Am. Ceram. Soc., 46 [2], 74-6 (1963).

0 0 0 0 4 6 0 7 6 0 4

APPENDIX (I)

Impurity analysis of Union Carbide Alumina single crystals, Englehard Co. "Amersil", Alcoa XA-16 reactive α-Al_2O_3 and "Baker Analyzed" Reagent $CaCo_3$ reported in weight percent of the oxides of the impurity elements indicated. "P.C." indicates "Principal Constituent".

Impurity	Sapphire*	XA-16**	Amersil*	$CaCo_3$**
Al	P.C.	P.C.	0.045	-
Ba	0.001	-	-	0.002
Na	0.050	0.080	-	0.002
Ca	0.001	0.030	0.0005	P.C.
Mg	0.0005	0.050	0.0007	0.020
Fe	0.004	0.010	0.015	0.001
Sn	0.005	-	-	-
B	0.005	0.001	-	-
Mn	-	0.0015	-	-
Cu	0.0005	-	0.0005	-
Ti	0.001	-	-	-
Si	0.210	0.050	P.C.	-
Cr	-	0.0002	-	-
Sr	-	-	-	0.020
Cl	-	-	-	0.0005
XF	-	-	-	0.0002
Pb	-	-	-	0.001
K	-	-	-	0.007
TOTALS	0.278	0.2227	0.0617	0.0537

Corning 7940 fused silica was produced by hydrolyzation of $SiCl_4$ when sprayed into an oxygen-hydrogen flame. While practically free form metallic impurities, it contains a high amount of OH($\simeq$1000 ppm) and Cl($\simeq$100 ppm).

*Spectrographic Analysis by American Spectrographic Laboratories, San Francisco, California.

**Chemical analysis by parent company.

APPENDIX II: Sample Computer Input/Output of X-ray Data for Lattice Parameter Lease Squares Refinement.

```
        SAMPLE 1A, I2 HR. HOLD AT 1805 CENTIGRADE
3000010000000000
 7.56149 7.68746 2.89409 90.      90.      90.
 1.54050
  4  2  2  88.899          1
  8  4  0  130.480         1
  7  6  0  137.760         1
1000000000000000 0
1000000000000000 0
1000000000000000 0
0100000000000000 0
0100000000000000 0
0100000000000000 0
0010000000000000 0
0010000000000000 0
0010000000000000 0
```

```
      SAMPLE 1A, I2 HR. HOLD AT 1805 CENTIGRADE

CONTROL CARD
      3  0  0  0  0  1  0  0  0  0  0  0  0  0  0  0  0  0

INITIAL DIRECT LATTICE CONSTANTS
        A =    7.56149                ALPHA =   90.00000
        B =    7.68746                 BETA =   90.00000
        C =    2.89409                GAMMA =   90.00000

INITIAL DIRECT LATTICE CONSTANTS
        A =     .13225                ALPHA =   90.00000
        B =     .13008                 BETA =   90.00000
        C =     .34553                GAMMA =   90.00000

WAVE LENGTHS
    1     1.54050
```

SAMPLE 1A, I2 HR. HOLD AT 1805 CENTIGRADE

INPUT DATA

H	K	L	LAMBDA	OBSERVATION	THETA(OBS)	D(OBS)	Q(OBS)	SIGMA(Q)	CORRECTION TERMS
4	2	2	1	88.899	44.449	1.09992	.82657	1.68522	
8	4	0	1	130.480	65.240	.84823	1.38987	1.28207	
7	6	0	1	137.760	68.880	.82572	1.46669	1.13308	

SAMPLE 1A, I2 HR. HOLD AT 1805 CENTIGRADE

OBSERVED AND CALCULATED INTERPLANAR SPACINGS, D, BASED ON INPUT PARAMETERS TO CYCLE 1

					RESIDUALS OF D		RESIDUALS OF Q	
H	K	L	D(OBS)	D(CALC)	(OBS-CALC)	(OBS-CALC)/SIGMA	(OBS-CALC)	(OBS-CALC)/SIGMA
4	2	2	1.09992	1.10090	-.00099	-.00088	.00148	.00088
8	4	0	.84823	.84816	.00007	.00017	-.00022	-.00017
7	6	0	.82572	.82586	-.00015	-.00046	.00053	.00046

SAMPLE 1A, I2 HR. HOLD AT 1805 CENTIGRADE

DISCREPANCY FACTORS BASED ON REFINED PARAMETERS AFTER CYCLE 1

```
NUMBER OF OBSERVATIONS (M) =    3
NUMBER OF VARIED PARAMETERS (N) =  1

FACTORS FOR D
   SUM (W*(OBS-CALC)**2) = 9.27075E-07
   SQRT(SUM(W*(OBS-CALC)**2)/M-N) = 6.80836E-04

FACTORS FOR Q
   SUM (W*(OBS-CALC)**2) = 9.25347E-07
   SQRT(SUM(W*(OBS-CALC)**2)/M-N) = 6.80201E-04
```

SAMPLE 1A, 12 HR. HOLD AT 1805 CENTIGRADE

OBSERVED AND CALCULATED INTERPLANAR SPACINGS, D, BASED ON REFINED PARAMETERS AFTER CYCLE 1

					RESIDUALS OF D		RESIDUALS OF Q	
H	K	L	D(OBS)	D(CALC)	(OBS-CALC)	(OBS-CALC)/SIGMA	(OBS-CALC)	(OBS-CALC)/SIGMA
4	2	2	1.09992	1.10086	-.00094	-.00084	.00141	.00084
8	4	0	.84823	.84807	.00015	.00039	-.00050	-.00039
7	6	0	.82572	.82580	-.00009	-.00027	.00031	.00027

SAMPLE 1A, 12 HR. HOLD AT 1805 CENTIGRADE

DIRECT LATTICE CONSTANTS AFTER LEAST-SQUARES CYCLE 1

PARAMETER	OLD	CHANGE	NEW	ERROR
A (ANG.)	7.56149	-.00097	7.56052	.00220
B (ANG.)	7.68746		7.68746	
C (ANG.)	2.89409		2.89409	
ALPHA (DEG.)	90.00000		90.00000	
BETA (DEG.)	90.00000		90.00000	
GAMMA (DEG.)	90.00000		90.00000	
UNIT CELL VOLUME (CUBIC ANG.)	168.2296	-.0216	168.2079	.0490

DIRECT LATTICE CONSTANT VARIANCE-COVARIANCE MATRIX

	A(ANG.)	B(ANG.)	C(ANG.)	ALPHA(RAD.)	BETA(RAD.)	GAMMA(RAD.)
A	4.853552E-06	0.	0.	0.	0.	0.
B		0.	0.	0.	0.	0.
C			0.	0.	0.	0.
ALPHA				0.	0.	0.
BETA					0.	0.
GAMMA						0.

DIRECT LATTICE CONSTANT CORRELATION MATRIX

	A	B	C	ALPHA	BETA	GAMMA
A	1.000000	0.000000	0.000000	0.000000	0.000000	0.000000
B		1.000000	0.000000	0.000000	0.000000	0.000000
C			1.000000	0.000000	0.000000	0.000000
ALPHA				1.000000	0.000000	0.000000
BETA					1.000000	0.000000
GAMMA						1.000000

SAMPLE 1A, 12 HR. HOLD AT 1805 CENTIGRADE

DISCREPANCY FACTORS BASED ON INPUT PARAMETERS TO CYCLE 1

NUMBER OF OBSERVATIONS (M) = 3
NUMBER OF VARIED PARAMETERS (N) = 1

FACTORS FOR D
SUM (W*(OBS-CALC)**2) = 1.01741E-06
SQRT(SUM(W*(OBS-CALC)**2)/M-N) = 7.13237E-04

FACTORS FOR Q
SUM (W*(OBS-CALC)**2) = 1.01523E-06
SQRT(SUM(W*(OBS-CALC)**2)/M-N) = 7.12470E-04

SAMPLE 1A, 12 HR. HOLD AT 1805 CENTIGRADE

PARAMETER SHIFTS, LEAST-SQUARES CYCLE 1

PARAMETER	OLD	CHANGE	NEW	ERROR
A *	.132249	.000017	.132266	.000039
B *	.130082		.130082	
C *	.345532		.345532	
ALPHA *	90.00000		90.00000	
BETA *	90.00000		90.00000	
GAMMA *	90.00000		90.00000	

ESTIMATED STANDARD ERROR OF UNIT WEIGHT OBSERVATION OF Q, BASED ON REFINEMENT OF 1 PARAMETERS
SQRT(SUM(W*(OBS-CALC)**2)/M-N) = .00068

APPENDIX III: Sample Computer Input/Output of Microprobe Data.

```
 5.01.   29 APR 76   VICTOR F DRAPER       5.01.748, 1700 C
                     MICRCPROBE ANALYSIS   5.01.

                                                    29 APR 76

NO. OF ELEMENTS = 3
 0 DEADTIME READINGS PER SET
 1 SAMPLE READINGS PER SET
BACKGRCUND READING METHOD = 1
SIGMA FOR STANCARD PEAK MAY NOT EXCEED  9.0 * SQRTF(N)
```

ELEMENT	ATOMIC NUMBER	PER CENT W OF STANCARD	TAU	OXYGEN FACTOR	SILICON FACTOR	
1	14	46.745000	2.000E-06	1.13931	0.	SIO2
2	13	52.925000	2.000E-06	.88947	0.	AL203
3	20	9.820000	2.000E-06	.85880	0.	ANORT

MICROPROBE ANALYSIS 5.01. PAGE 1
29 APR 76

INPUT DATA

	NAME	TIME	CURRENT	SPEC 1	SPEC 2	SPEC 3	KODE
1		10.00	-0.	33954	38	4	213233
1		10.00	-0.	33598	65	2	213233
1		10.00	-0.	33547	55	2	213233
1		10.00	-0.	33239	67	2	213233
1		10.00	-0.	32768	32	6	213233
1		10.00	-0.	31905	61	11	213233
1		10.00	-0.	32077	46	3	213233
2		10.00	-0.	32	34027	2	312233
2		10.00	-0.	46	33544	1	312233
2		10.00	-0.	42	33334	4	312233
2		10.00	-0.	36	33103	2	312233
2		10.00	-0.	32	33706	4	312233
2		10.00	-0.	30	33804	2	312233
3		10.00	-0.	15882	8202	2274	313223
3		10.00	-0.	15484	8132	2192	313223
3		10.00	-0.	15480	8065	2263	313223
3		10.00	-0.	13296	8602	2463	313223
3		10.00	-0.	16294	8702	2463	313223
3		10.00	-0.	16771	8602	2581	313223
3		10.00	-0.	17190	8844	2563	313223
3		10.00	-0.	17411	8633	2443	313223
4	INTERFC	10.00	-0.	20	23929	9	010203
5		10.00	-0.	75	23627	13	010203
6		10.00	-0.	74	23714	11	010203
7		10.00	-0.	55	23618	8	010203
8		10.00	-0.	54	23648	7	010203
9		10.00	-0.	47	23519	5	010203
10		10.00	-0.	47	23410	9	010203
11		10.00	-0.	57	23102	2	010203
12		10.00	-0.	42	23139	4	010203
13		10.00	-0.	54	23060	8	010203
14		10.00	-0.	49	22679	5	010203
15		10.00	-0.	41	22887	8	010203
16		10.00	-0.	46	22892	2	010203
17		10.00	-0.	61	22610	6	010203
18		10.00	-0.	54	22504	7	010203
19		10.00	-0.	32	22249	3	010203
20		10.00	-0.	66	22043	8	010203
21		10.00	-0.	47	21935	8	010203
22		10.00	-0.	42	21735	10	010203
23		10.00	-0.	65	21674	1	010203
24		10.00	-0.	68	21599	4	010203
25		10.00	-0.	54	21445	5	010203
26		10.00	-0.	1660	19308	5	010203
27		10.00	-0.	2733	17777	6	010203
28		10.00	-0.	2859	17833	10	010203
29		10.00	-0.	2984	17650	4	010203
30		10.00	-0.	2998	17600	10	010203
31		10.00	-0.	2974	17512	8	010203
32		10.00	-0.	3048	17228	6	010203
33		10.00	-0.	3098	17633	6	010203
34		10.00	-0.	3001	17433	3	010203
35		10.00	-0.	3077	17338	6	010203
36		10.00	-0.	3190	17477	8	010203
37		10.00	-0.	3280	17464	6	010203
38		10.00	-0.	3302	17427	3	010203

MICROPROBE ANALYSIS 5.01. PAGE 2
29 APR 76

AVERAGED DATA

		REL. TIME	CURRENT	SPECTROMETER 1 CTS/SEC	SIGMA		SPECTROMETER 2 CTS/SEC	SIGMA		SPECTROMETER 3 CTS/SEC	SIGMA	
1		70	0.	3301.3	27.6	2 1	5.2	.5	3 2	.4	.1	3 3
2		60	0.	3.6	.2	3 1	3358.6	12.4	2 2	.2	.1	3 3
3		80	0.	1597.6	43.2	3 1	847.3	9.7	3 2	240.5	4.8	2 3
4	INTERFC	10	-0.	2.0	.4	0 1	2392.9	15.5	0 2	.9	.3	0 3
5		10	-0.	7.5	.9	0 1	2362.7	15.4	0 2	1.3	.4	0 3
6		10	-0.	7.4	.9	0 1	2371.4	15.4	0 2	1.1	.3	0 3
7		10	-0.	5.5	.7	0 1	2361.8	15.4	0 2	.8	.3	0 3
8		10	-0.	5.4	.7	0 1	2364.8	15.4	0 2	.7	.3	0 3
9		10	-0.	4.7	.7	0 1	2351.9	15.3	0 2	.5	.2	0 3
10		10	-0.	4.7	.7	0 1	2341.0	15.3	0 2	.9	.3	0 3
11		10	-0.	5.7	.8	0 1	2310.2	15.2	0 2	.2	.1	0 3
12		10	-0.	4.2	.6	0 1	2313.9	15.2	0 2	.4	.2	0 3
13		10	-0.	5.4	.7	0 1	2306.0	15.2	0 2	.8	.3	0 3
14		10	-0.	4.9	.7	0 1	2267.9	15.1	0 2	.5	.2	0 3
15		10	-0.	4.1	.6	0 1	2288.7	15.1	0 2	.8	.3	0 3
16		10	-0.	4.6	.7	0 1	2289.2	15.1	0 2	.2	.1	0 3
17		10	-0.	6.1	.8	0 1	2261.0	15.0	0 2	.6	.2	0 3
18		10	-0.	5.4	.7	0 1	2250.4	15.0	0 2	.7	.3	0 3
19		10	-0.	3.2	.6	0 1	2224.9	14.9	0 2	.3	.2	0 3
20		10	-0.	6.6	.8	0 1	2204.3	14.8	0 2	.8	.3	0 3
21		10	-0.	4.7	.7	0 1	2193.5	14.8	0 2	.8	.3	0 3
22		10	-0.	4.2	.6	0 1	2173.5	14.7	0 2	1.0	.3	0 3
23		10	-0.	6.5	.8	0 1	2167.4	14.7	0 2	.1	.1	0 3
24		10	-0.	6.8	.8	0 1	2159.9	14.7	0 2	.4	.2	0 3
25		10	-0.	5.4	.7	0 1	2144.5	14.6	0 2	.5	.2	0 3
26		10	-0.	166.0	4.1	0 1	1930.8	13.9	0 2	.5	.2	0 3
27		10	-0.	273.3	5.2	0 1	1777.7	13.3	0 2	.6	.2	0 3
28		10	-0.	285.9	5.3	0 1	1783.3	13.4	0 2	1.0	.3	0 3
29		10	-0.	298.4	5.5	0 1	1765.0	13.3	0 2	.4	.2	0 3
30		10	-0.	299.8	5.5	0 1	1760.0	13.3	0 2	1.0	.3	0 3
31		10	-0.	297.4	5.5	0 1	1751.2	13.2	0 2	.8	.3	0 3
32		10	-0.	304.8	5.5	0 1	1722.8	13.1	0 2	.6	.2	0 3
33		10	-0.	309.8	5.6	0 1	1763.3	13.3	0 2	.6	.2	0 3
34		10	-0.	300.1	5.5	0 1	1743.3	13.2	0 2	.3	.2	0 3
35		10	-0.	307.7	5.5	0 1	1733.8	13.2	0 2	.6	.2	0 3
36		10	-0.	319.0	5.6	0 1	1747.7	13.2	0 2	.8	.3	0 3
37		10	-0.	328.0	5.7	0 1	1746.4	13.2	0 2	.6	.2	0 3
38		10	-0.	330.2	5.7	0 1	1742.7	13.2	0 2	.3	.2	0 3
39		10	-0.	314.2	5.6	0 1	1734.3	13.2	0 2	.6	.2	0 3
40		10	-0.	330.4	5.7	0 1	1767.5	13.3	0 2	.4	.2	0 3
41		10	-0.	310.7	5.6	0 1	1749.2	13.2	0 2	.6	.2	0 3
42		10	-0.	319.6	5.7	0 1	1755.6	13.2	0 2	1.1	.3	0 3
43		10	-0.	324.2	5.7	0 1	1738.3	13.2	0 2	.5	.2	0 3
44		10	-0.	325.8	5.7	0 1	1767.0	13.3	0 2	.7	.3	0 3
45		10	-0.	318.5	5.6	0 1	1759.5	13.3	0 2	.6	.2	0 3
46		10	-0.	340.3	5.8	0 1	1766.6	13.3	0 2	.9	.3	0 3
47		10	-0.	317.6	5.6	0 1	1730.5	13.2	0 2	.6	.2	0 3
48		10	-0.	330.7	5.8	0 1	1764.5	13.3	0 2	.5	.2	0 3
49		10	-0.	335.6	5.8	0 1	1774.9	13.3	0 2	1.2	.3	0 3
50		10	-0.	314.9	5.6	0 1	1781.8	13.3	0 2	.5	.2	0 3
51		10	-0.	333.2	5.8	0 1	1743.6	13.2	0 2	.3	.2	0 3
52		10	-0.	334.5	5.8	0 1	1751.7	13.2	0 2	1.3	.4	0 3
53		10	-0.	361.8	6.0	0 1	1735.8	13.2	0 2	1.5	.4	0 3
54		10	-0.	399.2	6.3	0 1	1664.8	12.9	0 2	1.9	.4	0 3

MICROPROBE ANALYSIS 5.01.

29 APR 76

ELEMENT	WEIGHT PERCENT	ATOMIC PERCENT	K-RATIO	INTENSITIES UNKN	INTENSITIES STD	BACKGROUNDS UNKN	BACKGROUNDS STD	ITER	OBS
SI KA	.01	.00	.0001	3	37220	34	34		
AL KA	40.38	28.66	.7268	25084	34511	48	48		
CA KA	.02	.01	.0020	5	2529	4	4		
O Ξ	59.59	71.33							
								3	1
SI KA	.07	.05	.0011	41	37220	34	34		
AL KA	39.91	28.27	.7172	24751	34511	48	48		
CA KA	.03	.02	.0036	9	2529	4	4		
O Ξ	59.98	71.66							
								3	2
SI KA	.07	.05	.0011	40	37220	34	34		
AL KA	40.04	28.38	.7200	24847	34511	48	48		
CA KA	.03	.01	.0028	7	2529	4	4		
O Ξ	59.86	71.56							
								3	3
SI KA	.04	.03	.0006	21	37220	34	34		
AL KA	39.90	28.25	.7169	24741	34511	48	48		
CA KA	.02	.01	.0016	4	2529	4	4		
O Ξ	60.05	71.71							
								3	4
SI KA	.04	.02	.0005	20	37220	34	34		
AL KA	39.95	28.29	.7179	24774	34511	48	48		
CA KA	.01	.01	.0012	3	2529	4	4		
O Ξ	60.01	71.68							
								3	5
SI KA	.02	.02	.0003	13	37220	34	34		
AL KA	39.75	28.12	.7137	24632	34511	48	48		
CA KA	.00	.00	.0004	1	2529	4	4		
O Ξ	60.22	71.86							
								3	6
SI KA	.02	.02	.0003	13	37220	34	34		
AL KA	39.59	27.98	.7103	24512	34511	48	48		
CA KA	.02	.01	.0020	5	2529	4	4		
O Ξ	60.38	71.99							
								3	7
SI KA	.04	.03	.0006	23	37220	34	34		
AL KA	39.10	27.58	.7004	24173	34511	48	48		
CA KA	.00	.00	.0002	0	2529	4	4		
O Ξ	60.86	72.39							
								3	8
SI KA	.01	.01	.0002	8	37220	34	34		
AL KA	39.16	27.63	.7016	24214	34511	48	48		
CA KA	.00	.00	.0002	0	2529	4	4		
O Ξ	60.82	72.36							
								3	9
SI KA	.04	.02	.0005	20	37220	34	34		
AL KA	39.04	27.53	.6991	24127	34511	48	48		
CA KA	.02	.01	.0016	4	2529	4	4		
O Ξ	60.91	72.44							
								3	10

Ξ DETERMINED BY DIFFERENCE

MICROPROBE ANALYSIS 5.01.

29 APR 76

SUBMITTED BY= VICTOR F CRAPER

DESCRIPTION= 5.01.74B, 1700 C

MEAN CHEMICAL COMPOSITION AND TWO
SIGMA LIMITS BASED ON 112 ANALYSES

ELEMENT	WEIGHT PERCENT	ATOMIC PERCENT
SI	13.22 +- 1.94	9.05 +- 1.35
AL	22.31 +- 2.14	15.66 +- 1.48
CA	1.83 +- .36	.88 +- .18
O Ξ	62.63 +- .64	74.41 +- .49

Ξ DETERMINED BY DIFFERENCE

MEAN INTENSITY RATIOS AND TWO SIGMA LIMITS

ELEMENT	K
SI KA	.2434 +- .0373
AL KA	.3949 +- .0382
CA KA	.1855 +- .0370

ACCELERATING VOLTAGE 15.0 KEV

X-RAY EMERGENCE ANGLE 41.0 DEGREES

PEAK-TO-BACKGROUND RATIOS (P/B), SENSITIVITIES
(SENS), AND MINIMUM DETECTABILITY LIMITS (MDL)

ELEMENT	P/B	SENS	MDL
SI	2655/1	.06 0/0	27 PPM
AL	1637/1	.09 0/0	37 PPM
CA	7045/1	.04 0/0	24 PPM

MICROPROBE ANALYSIS 5.01.

29 APR 76

CORRECTIONS

ELEMENT	BACKSCATTER	IONIZATION-ABSORPTION	FLOURESCENCE	TOTAL	
SI KA	.973	1.056	1.384	1.000	1.421
AL KA	.980	1.078	1.228	.995	1.290
CA KA	.940	1.127	1.334	1.000	1.395

+++NOTE+++

SI DETERMINED RELATIVE TO A STANDARD OF SILICA

AL DETERMINED RELATIVE TO A STANDARD OF ALUMINA

CA DETERMINED RELATIVE TO A STANDARD OF ANORTHITE

OBS PTS	MICRON STEP	$$$$ CONCENTRATION $$$$$ SI+4	AL+3	CA+2	$$$$$$$$ WEIGHT PERCENT $$$$$$$$$ SIO2	AL2O3	CAO	TOTAL	$$ NORMALIZED WT PCT $$$ SIO2	AL2O3	CAO	DENSITY
1	0.	.00	3.96	.00	.01	76.30	.03	76.34	.02	99.95	.04	3.97
2	1.00	.01	3.95	.00	.16	75.40	.05	75.61	.21	99.73	.06	3.97
3	2.00	.01	3.96	.00	.15	75.66	.04	75.85	.20	99.75	.05	3.97
4	3.00	.00	3.96	.00	.08	75.39	.02	75.49	.11	99.86	.03	3.97
5	4.00	.00	3.96	.00	.08	75.47	.02	75.57	.10	99.88	.02	3.97
6	5.00	.00	3.96	.00	.05	75.10	.01	75.16	.07	99.93	.01	3.97
7	6.00	.00	3.96	.00	.05	74.78	.03	74.86	.07	99.90	.04	3.97
8	7.00	.00	3.96	.00	.09	73.88	.00	73.97	.12	99.88	.00	3.97
9	8.00	.00	3.96	.00	.03	74.00	.00	74.03	.04	99.96	.00	3.97
10	9.00	.00	3.96	.00	.08	73.76	.02	73.86	.10	99.87	.03	3.97
11	10.00	.00	3.96	.00	.06	72.65	.01	72.71	.08	99.91	.01	3.97
12	11.00	.00	3.96	.00	.03	73.26	.02	73.31	.04	99.93	.03	3.97
13	12.00	.00	3.96	.00	.05	73.27	.00	73.32	.06	99.93	.00	3.97
14	13.00	.01	3.96	.00	.10	72.44	.01	72.56	.14	99.84	.01	3.97
15	14.00	.00	3.96	.00	.08	72.13	.02	72.23	.11	99.87	.02	3.97
16	15.00	.00	3.96	.00	.01	71.39	.00	71.41	.02	99.98	.00	3.97
17	16.00	.01	3.96	.00	.12	70.77	.02	70.92	.17	99.80	.03	3.97
18	17.00	.00	3.96	.00	.05	70.46	.02	70.53	.07	99.90	.03	3.97
19	18.00	.00	3.96	.00	.03	69.88	.03	69.94	.04	99.91	.05	3.97
20	19.00	.01	3.96	.00	.12	69.69	.00	69.81	.17	99.83	.00	3.97
21	20.00	.01	3.96	.00	.13	69.47	.00	69.60	.18	99.81	.00	3.97
22	21.00	.00	3.96	.00	.08	69.02	.01	69.10	.11	99.88	.01	3.97
23	22.00	.35	3.62	.00	5.98	62.10	.01	68.09	8.79	91.20	.01	3.97
24	23.00	.58	3.39	.00	9.77	57.19	.01	66.97	14.59	85.40	.02	3.97
25	24.00	.60	3.36	.00	10.23	57.32	.03	67.58	15.13	84.82	.05	3.97
26	25.00	.63	3.34	.00	10.66	56.74	.00	67.39	15.81	84.18	.00	3.97
27	26.00	.63	3.33	.00	10.70	56.58	.03	67.32	15.90	84.05	.05	3.97
28	27.00	.63	3.34	.00	10.61	56.33	.02	66.96	15.84	84.12	.03	3.97
29	28.00	.65	3.32	.00	10.85	55.45	.01	66.31	16.36	83.63	.02	3.97
30	29.00	.65	3.32	.00	11.06	56.65	.01	67.72	16.34	83.65	.02	3.97
31	30.00	.64	3.33	.00	10.70	56.08	.00	66.78	16.02	83.98	.00	3.97
32	31.00	.65	3.31	.00	10.96	55.77	.01	66.74	16.42	83.56	.02	3.97
33	32.00	.67	3.30	.00	11.38	56.16	.02	67.55	16.84	83.13	.03	3.97
34	33.00	.68	3.28	.00	11.70	56.09	.01	67.80	17.25	82.73	.02	3.97
35	34.00	.69	3.28	.00	11.77	55.97	.00	67.75	17.38	82.62	.00	3.97
36	35.00	.66	3.30	.00	11.19	55.77	.01	66.97	16.71	83.27	.02	3.97
37	36.00	.68	3.28	.00	11.81	56.71	.00	68.52	17.23	82.77	.00	3.97
38	37.00	.65	3.31	.00	11.08	56.23	.01	67.32	16.46	83.52	.02	3.97
39	38.00	.67	3.30	.00	11.41	56.39	.04	67.83	16.82	83.13	.06	3.97
40	39.00	.68	3.29	.00	11.55	55.86	.01	67.42	17.14	82.85	.01	3.97
41	40.00	.68	3.29	.00	11.64	56.71	.02	68.37	17.03	82.95	.02	3.97
42	41.00	.66	3.30	.00	11.37	56.51	.01	67.89	16.75	83.23	.02	3.97
43	42.00	.70	3.26	.00	12.16	56.65	.03	68.84	17.66	82.30	.04	3.97
44	43.00	.67	3.29	.00	11.31	55.64	.01	66.97	16.89	83.09	.02	3.97
45	44.00	.68	3.28	.00	11.81	56.62	.01	68.44	17.26	82.73	.01	3.97
46	45.00	.69	3.27	.00	12.00	56.92	.04	68.96	17.40	82.54	.06	3.97
47	46.00	.65	3.31	.00	11.26	57.19	.01	68.46	16.46	83.54	.01	3.97
48	47.00	.69	3.27	.00	11.88	56.99	.00	67.87	17.50	82.49	.00	3.97
49	48.00	.69	3.27	.00	11.93	56.23	.05	68.21	17.50	82.43	.07	3.97
50	49.00	.74	3.22	.00	12.89	55.67	.06	68.62	18.79	81.13	.09	3.97
51	50.00	.13	.53	.00	14.13	53.44	.08	67.65	20.89	78.99	.12	.64
52	51.00	.14	.47	.00	15.45	51.44	.18	67.08	23.04	76.69	.27	.62
53	52.00	.16	.43	.00	17.77	48.64	.30	66.91	26.86	72.69	.44	.59
54	53.00	.17	.37	.00	20.35	44.56	.60	65.50	31.07	68.02	.91	.55
55	54.00	.18	.31	.01	23.21	39.94	.99	64.15	36.19	62.27	1.54	.50

This report was done with support from the United States Energy Research and Development Administration. Any conclusions or opinions expressed in this report represent solely those of the author(s) and not necessarily those of The Regents of the University of California, the Lawrence Berkeley Laboratory or the United States Energy Research and Development Administration.

0 0 0 0 4 5 0 2 2 9 4